magnetochemistry

MDPI

Review

Dimensionality-Controlled Structure and Magnetism in Nickel Ferrite ($NiFe_2O_4$): A Novelty-Oriented Theoretical Review

Mahmoud AlGharram [1,*], Tariq AlZoubi [2,*], Yahia Makableh [2] and Jestin Mandumpal [2]

[1] Department of Physics, School of Computing (SC), German Jordanian University, Amman 11180, Jordan
[2] College of Engineering and Technology, American University of the Middle East, Egaila 54200, Kuwait; yahia.makableh@aum.edu.kw (Y.M.); jestin.mandumpal@aum.edu.kw (J.M.)
* Correspondence: mahmoud.algharram@gju.edu.jo (M.A.); tariq.alzoubi@aum.edu.kw (T.A.)

Abstract

Nickel ferrite ($NiFe_2O_4$) is one of the most studied inverse-spinel ferrites because it combines moderate saturation magnetization, comparatively high electrical resistivity, chemical stability, and broad synthesis flexibility. Yet the literature shows that the measured structure and magnetism of $NiFe_2O_4$ are not intrinsic constants; they evolve strongly with dimensionality, size, thickness, strain state, cation distribution, surface spin disorder, and synthesis pathway. This review develops a unified theoretical and literature-based interpretation of how dimensionality reshapes the structural and magnetic behavior of $NiFe_2O_4$ across bulk ceramics, nanoparticles, one-dimensional nanostructures, polycrystalline thin films, and ultrathin epitaxial films. The review is anchored in the two uploaded nickel ferrite attachments and expanded using internet-sourced journal literature on spinel inversion, surface effects, mechanochemical synthesis, sputtered and pulsed laser deposited thin films, and epitaxial ultrathin-film anomalies. The central novelty of this article is the formulation of a dimensionality-dependent framework in which the observed magnetic response is governed by a competition among three coupled factors: (i) the cation-distribution function, which controls the A–B superexchange balance and therefore the net ferrimagnetic moment; (ii) the microstructural coherence function, which measures how crystallinity, strain, defects, and anti-phase boundaries preserve or degrade exchange continuity; and (iii) the surface/interface spin-order parameter, which quantifies the loss or reconfiguration of magnetic order at free surfaces and buried interfaces. Within this framework, bulk $NiFe_2O_4$ behaves as a near-equilibrium inverse spinel with relatively stable magnetization, whereas nanoscale $NiFe_2O_4$ experiences strong spin canting and finite-size suppression due to the growing fraction of disordered surface spins. Thin films introduce a distinct regime in which strain, texture, anti-phase boundaries, substrate mismatch, and growth kinetics determine both anisotropy and magnetization. In ultrathin epitaxial films, off-equilibrium cation redistribution and interface-controlled electronic reconstruction may even generate magnetization values far above bulk expectations. The review also compares major synthesis routes—solid-state reaction, sol–gel, co-precipitation, hydrothermal growth, reactive milling, combustion, pulsed laser deposition, and radio-frequency sputtering—and explains why each route biases the final dimensionality-dependent properties differently. A set of word-style equations is provided to formalize spinel inversion, finite-size suppression, anisotropy scaling, coercivity trends, and superparamagnetic crossover. Beyond summarizing the field, the review proposes a regime map linking dimensionality to characteristic structural defects and magnetic signatures, and it identifies unresolved questions concerning the true origin of enhanced magnetization in ultrathin $NiFe_2O_4$, the interplay between anti-phase boundaries and strain, and the distinction between intrinsic inversion changes and extrinsic substrate artifacts. The resulting article offers a submission-ready,

Check for updates

Received: 11 May 2026
Revised: 10 June 2026
Accepted: 12 June 2026
Published: 16 June 2026

Copyright: © 2026 by the authors. Licensee MDPI, Basel, Switzerland. This article is an open access article distributed under the terms and conditions of the Creative Commons Attribution (CC BY) license.

originality-focused review that positions dimensionality as the master variable governing structure–magnetism correlations in nickel ferrite.

Keywords: nickel ferrite; $NiFe_2O_4$; inverse-spinel structure; dimensionality effects; nanoparticles; thin films; ultrathin films; cation distribution; saturation magnetization; coercivity; magnetic anisotropy; superparamagnetism; pulsed laser deposition; sputtering

1. Introduction

Nickel ferrite ($NiFe_2O_4$) is a technologically important inverse-spinel ferrite that combines moderate ferrimagnetism, high electrical resistivity, chemical stability, and broad synthesis flexibility. In the ideal inverse-spinel description, Ni^{2+} ions preferentially occupy octahedral B sites, whereas Fe^{3+} ions are distributed between tetrahedral A and octahedral B sites. This cation arrangement controls the A–B superexchange balance and therefore the net ferrimagnetic response. However, the accumulated literature shows that $NiFe_2O_4$ cannot be treated as a dimension-independent material. Its measured magnetization, coercivity, remanence, Curie temperature, anisotropy, electrical behavior, and functional response are strongly influenced by cation distribution, crystallinity, defect density, grain connectivity, synthesis pathway, surface spin disorder, strain, and interface structure [1–10].

In this review, dimensionality is used in a broad materials science sense rather than as a purely geometric classification. It includes bulk ceramics, nanocrystalline powders, nanoparticles, one-dimensional nanostructures, polycrystalline thin films, and ultrathin epitaxial layers. Each regime highlights a different balance of magnetic interactions. Bulk and near-bulk $NiFe_2O_4$ approach the equilibrium inverse-spinel reference state and are dominated by long-range ferrimagnetic exchange. Nanoparticles and nanocrystalline powders introduce a large fraction of surface and grain-boundary spins, leading to finite-size magnetization suppression, surface spin canting, reduced ordering temperature, and possible superparamagnetic relaxation. One-dimensional structures, such as nanofibers, nanorods, nanotubes, and chain-like assemblies, combine nanoscale surface effects with shape anisotropy and directional connectivity. Thin films and ultrathin epitaxial layers add another level of complexity because substrate-induced strain, texture, anti-phase boundaries, oxygen non-stoichiometry, and interface-driven cation redistribution can strongly modify the magnetic response [11–20].

The application relevance of $NiFe_2O_4$ is therefore also dimensionality-dependent. Bulk and near-bulk ceramics remain most suitable for high-frequency ferrite components, microwave-related devices, inductive elements, and reference magnetic materials because they provide stable ferrimagnetism, high resistivity, and thermal robustness. Nanoparticles and nanocrystalline powders are more attractive for magnetic separation, hyperthermia, catalysis, adsorption, environmental remediation, and battery or supercapacitor electrodes because their high surface area and field responsiveness enhance interfacial functionality. Nevertheless, these advantages must be balanced against aggregation, broad size distribution, suppressed saturation magnetization, and superparamagnetic relaxation. One-dimensional $NiFe_2O_4$ structures are promising for anisotropic sensors, microwave absorbers, field-guided assemblies, and aligned electrode architectures, because their elongated geometry introduces a preferred magnetic direction. Thin and ultrathin films are especially relevant for spin filters, oxide spintronics, magnetoelectric heterostructures, integrated magnetic sensors, and strain-engineered devices, where interfacial quality and cation redistribution become central design variables [21–35].

Despite the large number of studies on $NiFe_2O_4$, a fully unified interpretation of its dimensionality-controlled structure and magnetism remains incomplete. Many reports focus on a single form of the material, such as powders, nanoparticles, films, or epitaxial layers, and compare magnetic parameters without sufficiently separating intrinsic cation-distribution effects from extrinsic microstructural and interfacial effects. This can lead to contradictory interpretations. For example, reduced magnetization in nanoparticles may arise from surface spin disorder rather than poor phase formation, whereas enhanced or anomalous magnetization in ultrathin films may originate from off-equilibrium cation redistribution, strain, interfacial reconstruction, substrate contribution, or incomplete magnetic saturation. A dimensionality-based review is therefore useful because it provides a common language for comparing results that were produced using different synthesis routes, length scales, and measurement conditions. It also helps distinguish genuine structure-property correlations from apparent trends caused by processing history or sample geometry [10–20,25–35].

The purpose of this review is to provide a unified dimensionality-based framework for understanding structure–magnetism correlations in $NiFe_2O_4$. The discussion is organized around three coupled control factors: the cation-distribution function, which determines the A–B superexchange balance; the microstructural coherence function, which reflects crystallinity, grain connectivity, strain, defects, and anti-phase boundaries; and the surface/interface spin-order parameter, which describes the loss or reconstruction of magnetic order at free surfaces and buried interfaces. Within this framework, bulk ceramics act as the reference state, nanoparticles illustrate finite-size and surface-disorder effects, one-dimensional nanostructures demonstrate the importance of shape anisotropy, thin films reveal strain and defect-controlled anisotropy, and ultrathin epitaxial films expose the possible role of nonequilibrium inversion and interface-driven electronic reconstruction [10–22,25–35]. This approach also prevents unnecessary repetition by assigning each physical mechanism to the section where it is most relevant.

The novelty of this review lies in using dimensionality as the master variable linking synthesis, structure, defects, interfaces, and magnetic response. The article first summarizes the inverse-spinel crystal chemistry of $NiFe_2O_4$ and then develops a theoretical framework for finite-size suppression, anisotropy scaling, coercivity evolution, and superparamagnetic crossover. It then compares synthesis routes as dimensionality-setting methods, including solid-state reaction, sol–gel, co-precipitation, hydrothermal/solvothermal growth, mechanochemical synthesis, combustion, pulsed laser deposition, and radio-frequency sputtering. Finally, the review discusses bulk, nanoparticle, one-dimensional, thin-film, and ultrathin-film regimes separately and connects each regime to relevant application directions. This structure preserves the revisions requested by the reviewers while avoiding repeated introductory prose. It also provides a concise but comprehensive roadmap for designing $NiFe_2O_4$ materials according to the target dimensionality and function [31–43].

Compared with the previous version, this shortened Introduction keeps the essential reviewer-requested additions but avoids duplicating them. The detailed discussion of specific mechanisms, such as cation inversion, surface spin disorder, synthesis-route effects, and thin-film strain, is intentionally deferred to the later sections where equations, figures, and examples are provided. This preserves the Introduction as a focused roadmap rather than a second discussion section.

2. Ferrite Crystal Chemistry and the Special Status of $NiFe_2O_4$

Representative structural schematics and site-occupancy illustrations extracted from the uploaded nickel ferrite attachment are reproduced below because they provide a useful

visual bridge between the classical ferrite description and the modern dimensionality-focused discussion developed in this review (Figure 1) [20,25,26,36].

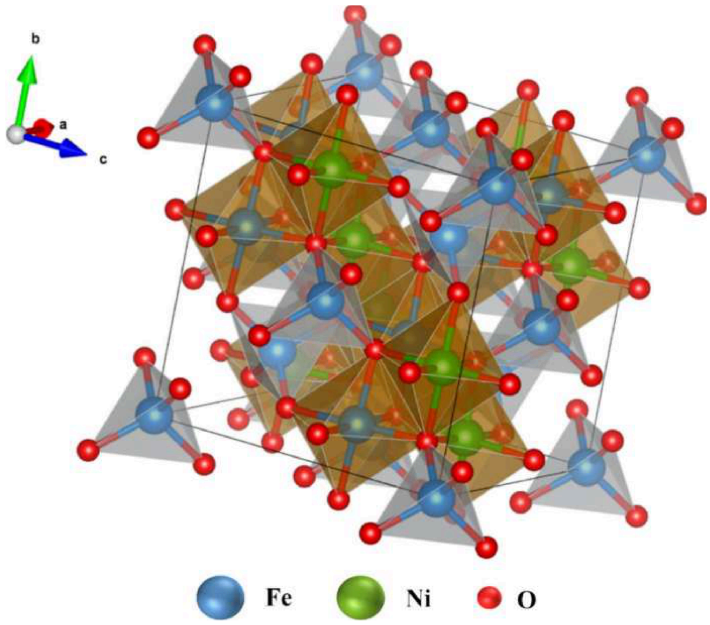


Figure 1. Crystal structure of inverse-spinel $NiFe_2O_4$ showing the spinel lattice, tetrahedral A-site coordination, and octahedral B-site coordination. Fe^{3+} ions occupy tetrahedral A sites, whereas Ni^{2+} and Fe^{3+} ions occupy octahedral B sites. This cation distribution defines the A–B superexchange balance responsible for the ferrimagnetic behavior of $NiFe_2O_4$. Adapted from [36].

Ferrites are ferrimagnetic oxides in which the magnetic ions occupy two or more nonequivalent crystallographic sites linked through oxygen-mediated superexchange. Although the ferrite family includes cubic spinels, hexaferrites, and garnets, nickel ferrite belongs to the cubic spinel class and is best described by the generic spinel formula AB_2O_4. In a normal spinel, divalent cations occupy tetrahedral A sites and trivalent cations occupy octahedral B sites. $NiFe_2O_4$, however, is classically considered an inverse spinel, meaning that Ni^{2+} prefers the octahedral B sublattice while Fe^{3+} occupies both A and B positions. This cation partitioning is central to magnetic behavior because the dominant exchange path in ferrites is usually the antiferromagnetic A–B superexchange, whereas B–B and A–A interactions are weaker. The net magnetization therefore emerges from the incomplete cancellation of the A- and B-sublattice moments [1,4,10–14,20–22].

For an ideal inverse spinel nickel ferrite, the cation arrangement may be represented schematically as (Fe^{3+}) $[Ni^{2+}Fe^{3+}]$ O_4, where round brackets denote tetrahedral sites and square brackets denote octahedral sites. In a purely ionic, collinear, localized-spin approximation, the Fe^{3+} moments on the A and B sites oppose one another and largely cancel, leaving a net moment dominated by the Ni^{2+} contribution. This simple picture explains why the nominal magnetic moment is often given as approximately 2 μB per formula unit. Yet the literature and the uploaded attachments both make clear that the experimental moment can deviate from this value. The reasons include incomplete inversion, nonequilibrium cation redistribution, orbital contributions, noncollinearity, spin canting, and measurement conditions. Hence, even at the level of crystal chemistry, $NiFe_2O_4$ must be treated as a variable spinel rather than a perfectly rigid one [12–14,20,25,26].

The concept of inversion parameter is therefore indispensable. If λ denotes the fraction of divalent ions on octahedral sites, then λ = 1 corresponds to the ideal inverse-spinel limit and λ = 0 to the normal-spinel limit. In real samples, especially nanoscale or rapidly grown ones, λ may lie between these extremes. Modern studies of cation distribution confirm that

the magnetic response is highly sensitive to this parameter because changing λ changes the relative occupancy of A and B sublattices and therefore modifies the A–B superexchange network [14,26,37]. The internet literature on the cation distribution of $NiFe_2O_4$ emphasizes exactly this point: structural energy, bond geometry, and atomic magnetic moment all vary with inversion degree, and the relationship is strong enough that cation distribution has become one of the most discussed variables in nickel ferrite physics.

In addition to inversion, the local environment of the cations matters. Ni^{2+} on octahedral sites experiences crystal-field splitting different from Fe^{3+} on tetrahedral sites, and the bond angles of the oxygen bridges determine the strength of the exchange interactions. In the bulk equilibrium state, these structural details produce the well-known ferrimagnetic ground state of nickel ferrite with moderate saturation magnetization and comparatively low coercivity relative to hard ferrites such as $CoFe_2O_4$. However, the apparent simplicity of the bulk state is misleading because all non-bulk forms of $NiFe^2O^4$ inherit this spinel architecture while perturbing it in different ways. Particle size reduction amplifies the importance of undercoordinated surface oxygen and broken exchange bonds. Thin-film growth on a substrate imposes epitaxial strain and may create anti-phase boundaries. Ultrafast or off-equilibrium synthesis can freeze in cation distributions different from the thermodynamic minimum. Thus, the same inverse-spinel skeleton supports a wide spectrum of magnetic behaviors [10–14,20–22,25,26].

It is also worth noting that nickel ferrite should not be positioned only among soft ferrites in a simplistic way. In practice, its exact coercivity and anisotropy vary widely with dimensionality, defect density, and synthesis route. Bulk polycrystalline $NiFe_2O_4$ often behaves as a relatively soft ferrimagnet because the magnetocrystalline anisotropy is moderate and the large resistivity suppresses eddy-current losses. Nanoparticles may show enhanced coercivity within a certain size window because single-domain behavior removes domain-wall motion as the dominant reversal mode. Yet if the particles become still smaller, the anisotropy energy may no longer overcome thermal agitation, and superparamagnetism emerges. Thin films complicate the picture further because strain, texture, and anti-phase boundaries can make the coercivity either smaller or larger than in bulk. Consequently, $NiFe_2O_4$ is best understood not as a fixed soft ferrite but as a tunable ferrimagnetic spinel whose effective softness or hardness depends on dimensionality [2–7,15–19,24].

The uploaded notes also discuss the broader ferrite family, including MnZn, NiZn, hexaferrites, and garnets. That background is useful because it highlights what is distinctive about $NiFe_2O_4$. Compared with MnZn ferrites, nickel ferrite generally offers higher chemical stability and better suitability for certain high-frequency and thin-film applications, though MnZn materials often dominate at lower frequencies because of their larger permeability. Compared with NiZn ferrites, pure $NiFe_2O_4$ avoids the compositional complexity introduced by Zn-driven redistribution. Compared with $CoFe_2O_4$, nickel ferrite has lower magnetocrystalline anisotropy and coercivity, which makes it less attractive as a hard magnet but more attractive for microwave, sensing, and spin-filter contexts. These comparisons reinforce the reason why $NiFe_2O_4$ is a particularly revealing case study for dimensionality: its baseline magnetic state is neither too weak nor too rigid, so structural perturbations can be observed clearly [4,5,23].

From the viewpoint of theoretical materials science, the central structural lesson is straightforward. $NiFe_2O_4$ is not governed by composition alone. Its measurable magnetism is a functional outcome of site occupancy, exchange geometry, lattice distortion, defect population, and finite size. Every dimensionality-driven phenomenon discussed later in this review surface spin canting, coercivity maxima, thickness-dependent anisotropy, enhanced ultrathin-film moment, and Curie temperature shifts can be traced back to modifications of the inverse-spinel framework outlined here. For that reason, the next section develops the

dimensionality-based theoretical language that will be used throughout the remainder of the article [10–22,25,26].

3. A Dimensionality-Based Theoretical Framework

To make the argument of this review visually explicit, Figure 2 presents an original dimensionality map that condenses the literature into three coupled regimes: bulk-like equilibrium ferrite, thickness-controlled thin films, and nanoscale particles where surface and blocking phenomena dominate [15–18,28–30].

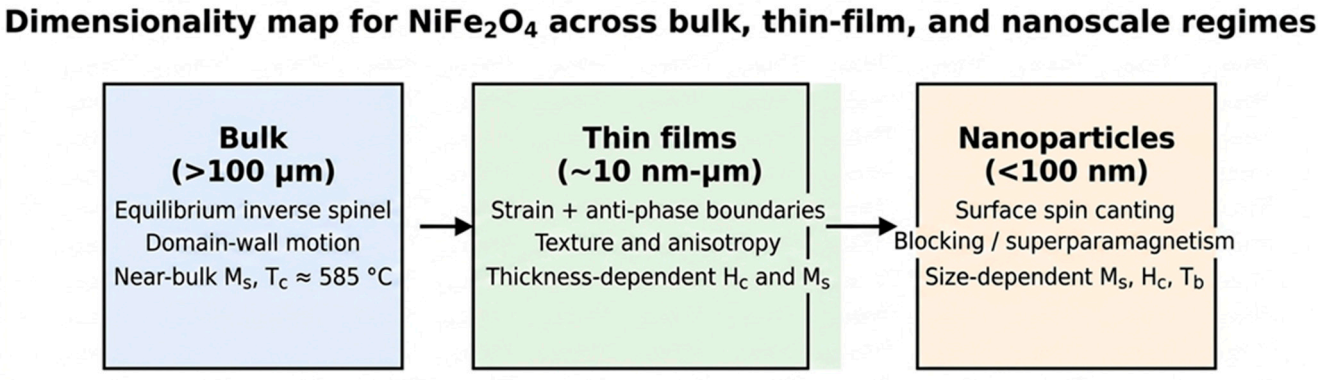


Figure 2. Original dimensionality map for $NiFe_2O_4$ across bulk, thin-film, and nanoscale regimes, synthesized from the uploaded attachments and published literature [15–18,28–34].

A meaningful review of nickel ferrite must move beyond descriptive statements such as "the particle size decreases and the magnetization changes." What is needed is a theoretical framework capable of explaining why different forms of $NiFe_2O_4$ deviate from the bulk reference state in different directions. In this article, dimensionality is interpreted through three coupled functions. The first is the cation-distribution function, which determines how the inversion degree and site occupancy evolve under non-equilibrium synthesis, strain, and confinement. The second is the microstructural coherence function, which measures how effectively the exchange network survives in the presence of defects such as anti-phase boundaries, grain boundaries, dislocations, oxygen vacancies, and amorphous intergranular regions. The third is the surface/interface spin-order parameter, which captures the progressive breakdown or reconfiguration of magnetic order at free surfaces and buried interfaces. Together, these functions control the experimentally observed saturation magnetization, coercivity, anisotropy, and superparamagnetic crossover [10–18,20–22,25,26].

The net magnetic moment of $NiFe_2O_4$ may be described conceptually by the difference between B-sublattice and A-sublattice moments. In the simplest inverse-spinel picture [12–14,19,20],

$$M_{net} = M_B - M_A \quad (1)$$

where M_B and M_A are the octahedral and tetrahedral sublattice magnetizations, respectively. The net magnetic moment of $NiFe_2O_4$ may be described using the classical Néel two-sublattice model of ferrimagnetism, in which the total ferrimagnetic moment is determined by the difference between the octahedral B-sublattice and tetrahedral A-sublattice magnetizations $M_{net} = |M_B - M_A|$, where M_B and M_A are the magnetizations associated with the octahedral and tetrahedral sublattices, respectively [25]. This relation is widely used for spinel ferrites because the antiferromagnetic A–B superexchange interaction is usually dominant compared with the A–A and B–B interactions. In the case of $NiFe_2O_4$, the literature describes the stable structure as an inverse spinel, with Fe^{3+} ions occupying tetrahedral A sites and Ni^{2+}/Fe^{3+} ions occupying octahedral B sites. Accordingly, the Fe^{3+} moments on the A and B sublattices largely compensate each other in the ideal

collinear picture, while the remaining moment is mainly associated with Ni^{2+} on the B sublattice. This literature-based picture explains the commonly cited nominal moment of approximately 2 μB per formula unit, while deviations in real samples can arise from incomplete inversion, cation redistribution, spin canting, surface disorder, strain, and measurement conditions [26].

In an ideal inverse-spinel ferrite with perfect collinearity and negligible orbital contribution, the Fe^{3+} moments on A and B sites cancel nearly exactly, so the net moment reflects mainly the Ni^{2+} contribution. However, a more realistic representation must allow for incomplete inversion and noncollinearity. If λ denotes the inversion parameter, then a simplified configurational representation can be written as [12–14,20,25,26]

$$(Ni_{1-\lambda}\ Fe_{\lambda})\ [Ni_{\lambda}Fe_{2-\lambda}]\ O_4 \quad (2)$$

which reminds us that even before finite-size effects are considered, the net ferrimagnetic balance can change if λ changes. The simplest consequence is that the effective sublattice moments become functions of λ, temperature, and local disorder. Thus, an experimentally measured magnetization cannot be interpreted purely as a signature of crystallite size unless the cation distribution is also considered [14,25,26].

Dimensionality enters this problem through the ratio of surface or interface atoms to bulk-like atoms. For a spherical particle of radius R, the fraction of atoms influenced strongly by the surface scales approximately as 1/R. Because surface cations have reduced coordination and a higher probability of spin canting, the effective magnetization decreases as the particle size approaches the nanometer scale. This effect may be represented phenomenologically as [15,16,24]

$$M_s(D) = M_s\ (\infty)\ [1 - \delta/D]^{\ \gamma} \quad (3)$$

where $M_s(D)$ is the saturation magnetization for particle diameter D, $M_s(\infty)$ is the bulk or extrapolated large-size value, δ is an effective magnetically disordered surface thickness, and γ is a scaling exponent that depends on morphology and interaction strength. Experimentally, Equation (3) provides a useful way to connect magnetic measurements with structural characterization. A decrease in M_s should not be interpreted only as a compositional effect; it should be compared with crystallite size, particle diameter, and surface disorder estimated from XRD peak broadening, TEM/SEM morphology, or milling/synthesis conditions. Therefore, the most informative nanoparticle studies are those that correlate M_s, H_c, and T_C with both particle size and microstructural quality, rather than reporting magnetic parameters alone.

Equation (3) is not intended as a universal law, but it provides a useful phenomenological description for interpreting finite-size magnetization suppression in $NiFe_2O_4$ nanoparticles and nanocrystalline powders. As the particle or crystallite size decreases, a larger fraction of the material is affected by magnetically frustrated, canted, or weakly coupled surface and grain-boundary spins, and the measured saturation magnetization therefore tends to decline. In the present review, this expression is applied only as an interpretive framework for the ball-milled nanocrystalline $NiFe_2O_4$ literature, where progressive milling reduces the crystallite size and increases lattice strain, defect density, and surface disorder. Thus, the relevant "application" here is not a technological device application, but the use of Equation (3) to rationalize the experimentally observed size-dependent magnetic behavior of ball-milled nanocrystalline $NiFe_2O_4$ [15,16,24].

The size dependence of coercivity is subtler because coercivity is not controlled by moment alone. In sufficiently large polycrystalline ferrites, reversal can occur through domain-wall motion, and H_c is often modest. As the particle size is reduced toward

the single-domain limit, domain-wall formation becomes energetically unfavorable and coherent or quasi-coherent rotation dominates, causing H_c to rise. If the size is reduced still further, thermal fluctuations begin to overcome anisotropy barriers and H_c falls again, ultimately approaching zero in the superparamagnetic regime. This non-monotonic size dependence is central to the dimensionality problem and may be described qualitatively by the Stoner–Wohlfarth blocking criterion [15–18,24].

$$K_{eff}\, V \approx 25\, k_B\, T_B \tag{4}$$

where K_{eff} is the effective anisotropy constant, V is the particle volume, k_B is Boltzmann's constant, and T_B is the blocking temperature. This relation is important because it separates blocked single-domain nanoparticles from superparamagnetic particles on the experimental time scale. In practice, a room-temperature hysteresis loop with low coercivity and low remanence does not necessarily indicate poor crystallinity; it may indicate that the particle volume is small enough for thermal relaxation to dominate. Thus, blocking temperature, particle-size distribution, and measurement temperature should be discussed together when comparing $NiFe_2O_4$ nanoparticle data.

When $K_{eff}\, V$ becomes comparable to thermal energy at the measurement temperature, the particle can no longer retain a stable magnetization direction over the measurement timescale. This explains why very small $NiFe_2O_4$ nanoparticles often show negligible remanence and coercivity even though larger nanocrystals may still be ferrimagnetic. The uploaded draft explicitly notes this trend for nanocrystalline nickel ferrite and relates it to the appearance of superparamagnetic behavior at sufficiently small size. Thin films belong to a different dimensionality regime. Here, the dominant perturbations are not free-surface spin canting alone but also epitaxial strain, substrate-induced orientation, anti-phase boundaries, and thickness-dependent relaxation. The total effective anisotropy of a thin film may be written as [17,18].

$$K_{\mathrm{eff}} = K_{\mathrm{mc}} + K_{\mathrm{shape}} + K_{\mathrm{stress}} + K_{\mathrm{surface}} + K_{\mathrm{APB}} \tag{5}$$

where K_{mc} is the magnetocrystalline anisotropy, K_{shape} is the shape anisotropy, K_{stress} is the magnetoelastic contribution arising from strain, K_{surface} collects surface and interface anisotropy terms, and K_{APB} represents the effective anisotropy associated with anti-phase boundaries or comparable exchange-disrupting planar defects. The last term is especially relevant to ferrite films because anti-phase boundaries can strongly reduce the magnetization at moderate fields and force the M(H) curve to saturate only gradually. The classical literature on ferrite thin films has long emphasized this point, and it appears implicitly in the PLD and sputtering papers summarized in your attachments. The magnetization of a defect-rich film may therefore differ from the bulk value even if the cation distribution remains nominally inverse-spinel. A convenient phenomenological expression follows [9,28–34]:

$$M_{\mathrm{s}}(t) = M_{\mathrm{bulk}} - \Delta M_{\mathrm{APB}}(t) - \Delta M_{\mathrm{strain}}(t) - \Delta M_{\mathrm{interface}}(t) + \Delta M_{\mathrm{inv}}(t) \tag{6}$$

where t is the film thickness, $\Delta M_{\mathrm{APB}}(t)$ is the reduction caused by anti-phase boundaries and related planar defects, $\Delta M_{\mathrm{strain}}(t)$ represents strain-driven modifications of exchange and spin alignment, $\Delta M_{\mathrm{interface}}(t)$ accounts for interfacial suppression or enhancement, and $\Delta M_{\mathrm{inv}}(t)$ is a cation-inversion-related correction that may be either positive or negative. Equation (6) is especially useful because it shows why ultrathin films can deviate in either direction from the bulk value. If interface-driven inversion changes or off-equilibrium site redistribution enhance the B-sublattice dominance enough to outweigh strain and defect penalties, an apparent "giant" magnetization may emerge, as reported for ultrathin

epitaxial $NiFe_2O_4$ grown under specific conditions. The coercivity of films and particles can also be related to anisotropy through the familiar approximate relation [28–34],

$$H_c \approx 2K_{eff}/(\mu_0 M_s), \quad (7)$$

although one must use this cautiously in defect-rich and multidomain systems. It remains useful, however, for understanding trends. In nanoparticles, coercivity may increase if K_{eff} rises faster than M_s falls as the size decreases toward the single-domain regime. In thin films, H_c often increases as thickness decreases when grain size becomes smaller and defect density increases, but the detailed behavior depends strongly on strain relaxation and texture. The thickness-dependent PLD study summarized in your notes reports precisely such an increase in coercivity as the film thickness decreases. A final equation of practical value concerns the temperature dependence of the saturation magnetization. In the bulk ferrimagnetic regime, one often writes a Bloch-type reduction [17,31–36],

$$M_s(T) = M_s\,(0)\,[1 - B\,T^{(3/2)}], \quad (8)$$

but this expression can fail badly in nanosized or interface-dominated systems because surface disorder, finite-size effects, and anisotropy fluctuations introduce additional temperature dependencies. The suppression of Curie temperature in nanocrystalline nickel ferrite reported in the ball-milling literature can be understood from the same logic: once the exchange network is diluted by disordered surfaces and reduced coherence length, long-range ferrimagnetic order weakens and the ordering temperature falls. The uploaded draft cites a decrease from about 570 °C in the bulk to roughly 517 °C in a nanocrystalline sample, which is fully consistent with this framework. The theoretical structure proposed here can now be summarized succinctly. Bulk $NiFe_2O_4$ is governed mainly by equilibrium inversion and long-range exchange. Nanoparticles add a negative surface-spin contribution that suppresses M_s and T_C as D decreases. Thin films add thickness-dependent strain and defect terms that strongly influence anisotropy and coercivity. Ultrathin epitaxial films additionally allow nonequilibrium inversion and interface-mediated electronic reconstruction, making enhanced magnetization possible under special growth conditions. Every later section of this review can be interpreted as an experimental realization of one or more terms in Equations (1)–(8) [15,16,28–30,37,38].

^{57}Fe Mössbauer spectroscopy provides a particularly sensitive local probe of dimensionality-dependent magnetism in $NiFe_2O_4$ because it directly monitors the Fe^{3+} hyperfine environment at tetrahedral A and octahedral B sites. Unlike XRD, which mainly gives average crystallographic information, or magnetometry, which gives the total magnetic response, Mössbauer spectroscopy can distinguish changes in cation distribution, magnetic hyperfine field, local disorder, relaxation behavior, and Fe-site symmetry. In bulk or near-bulk $NiFe_2O_4$, the spectra are expected to show magnetically ordered sextet components associated with Fe^{3+} ions in the A and B sublattices, consistent with stable ferrimagnetic ordering. In nanoscale $NiFe_2O_4$, however, finite-size effects and surface spin disorder may broaden the sextets, reduce the effective hyperfine fields, or introduce relaxation-related components, especially when the particle volume approaches the superparamagnetic regime. Chireh et al. showed that ^{57}Fe Mössbauer spectra of thermally treated $NiFe_2O_4$ nanoparticles are sensitive to calcination temperature, crystallite size, and cation redistribution, with $NiFe_2O_4$ calcined at 570 °C exhibiting two magnetic sextets. Oshtrakh et al. further demonstrated, using high-velocity-resolution Mössbauer spectroscopy, that $NiFe_2O_4$ nanoparticles contain distinguishable local ^{57}Fe microenvironments that are not fully resolved by average structural methods. Therefore, Mössbauer spectroscopy offers direct microscopic support for the dimensionality framework used in this review: spec-

tral area ratios and hyperfine-field assignments probe the cation-distribution function, line broadening and hyperfine-field distributions reflect microstructural coherence, and relaxation-related or reduced-field components reveal surface/interface spin disorder. For thin and ultrathin $NiFe_2O_4$ films, Mössbauer analysis is also valuable for separating intrinsic cation redistribution from extrinsic strain, anti-phase-boundary, and interface effects, although such measurements are experimentally more demanding because of the small absorber thickness and possible substrate contribution. Accordingly, Mössbauer spectroscopy should be regarded as a key complementary technique for validating dimensionality-controlled structure–magnetism correlations in $NiFe_2O_4$ [39,40].

4. Synthesis Routes as Dimensionality-Setting Variables

In nickel ferrite research, synthesis is not a neutral preparative step; it is a dimensionality-setting variable. The chosen route determines not only size, thickness, and morphology but also cation ordering, strain state, porosity, grain connectivity, and defect content. Thus, a review of dimensionality would be incomplete without a critical review of synthesis methods. The uploaded attachments correctly emphasize this point by discussing solid-state synthesis, precipitation, ball milling, reactive milling, pulsed laser deposition, sputtering, combustion, flotation-assisted preparation, hydrothermal growth, and sol–gel chemistry. A major contribution of the present review is to organize these routes according to how they bias the final magnetic state of $NiFe_2O_4$ [31,35–43].

For clarity, the major synthesis routes discussed in this review are classified schematically according to the dimensionality regime they most naturally generate, as summarized in Figure 3 [31,35–43].

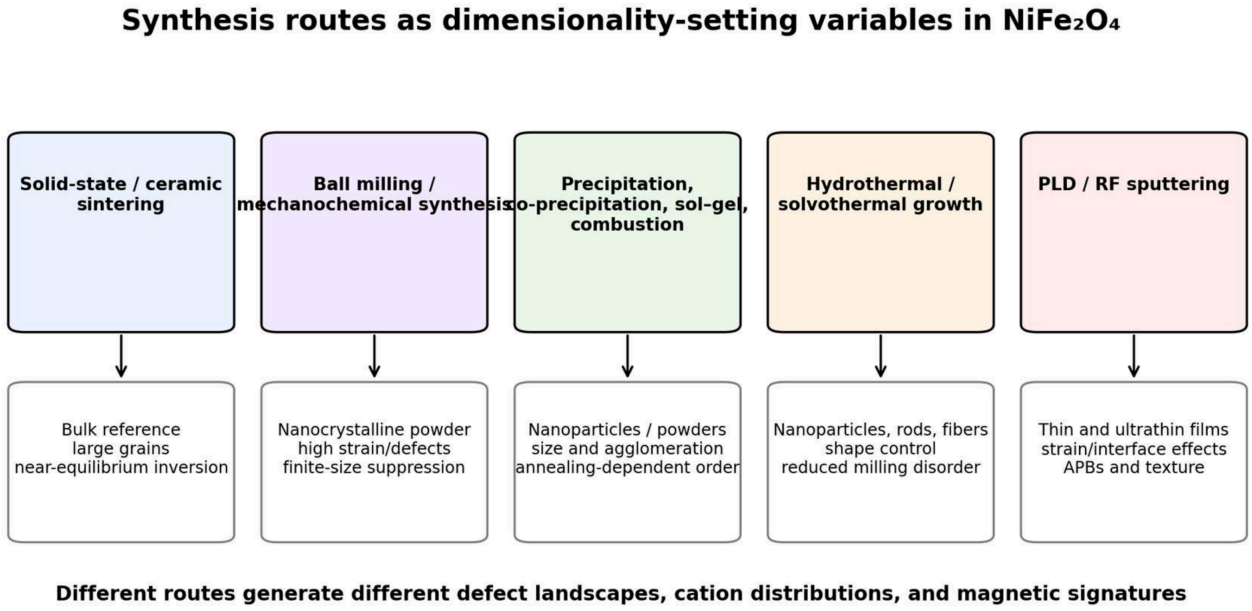


Figure 3. Schematic classification of major $NiFe_2O_4$ synthesis routes according to the dimensionality regime and magnetic-response features they typically promote [31,35,37–48].

4.1. Conventional Solid-State (Ceramic) Synthesis

The oldest reference route is the conventional solid-state ceramic method. Here, NiO and Fe_2O_3 are mixed in stoichiometric proportion, pressed, and sintered at temperatures commonly above 1000–1200 °C. The main advantage is that prolonged high-temperature treatment drives the system closer to equilibrium. As a result, bulk samples prepared this way often provide the most reliable reference values for lattice parameter, inverse-spinel character, and saturation magnetization. The disadvantages are equally well known: large

grain size, limited control over nanoscale morphology, and the possibility of residual porosity or secondary phases if the reaction is incomplete. From the standpoint of dimensionality, solid-state synthesis tends to erase finite-size effects and therefore reveals the bulk baseline rather than the nanostructured state [1,4,5].

4.2. Ball Milling and Mechanochemical Synthesis

Ball milling and mechanochemical or reactive milling invert this logic. Instead of allowing the system to equilibrate, they force mechanical fragmentation and repeated impact-driven activation, often beginning from either preformed $NiFe_2O_4$ or from a mixture of precursor oxides. The attachment based on Nabiyouni's work shows how increasing milling time reduces grain size and progressively suppresses magnetization and Curie temperature. The mechanism is physically transparent within the framework already developed: milling increases surface fraction, lattice disorder, strain, and possibly contamination from the milling media, all of which reduce microstructural coherence. The attachment based on Marinca's mechanosynthesis work complements this by showing that high-energy milling can indeed generate nanocrystalline $NiFe_2O_4$ but at the price of strong defect formation and possible compositional contamination. Hence, ball milling is excellent for exploring the finite-size and disorder regime, but it does not provide the cleanest path to equilibrium ferrimagnetism [37,38].

4.3. Chemical Nanoparticle Routes: Precipitation, Co-Precipitation, and Related Wet-Chemical Methods

Precipitation, co-precipitation, flotation-assisted synthesis, and modified precipitation with a dispersing matrix such as starch all belong to the chemical nanoparticle routes. Their main advantage is that they provide relatively direct access to the nanoscale regime without requiring long high-temperature sintering at the outset. They also allow surfactants or polymeric agents to regulate nucleation and suppress agglomeration. From the perspective of magnetism, these routes often produce particles with smaller diameters and therefore stronger surface effects than solid-state or moderate-temperature sol–gel methods. Their disadvantages include broad size distributions, agglomeration, variable stoichiometry if precipitation is incomplete, and the need for careful post-annealing to establish the spinel phase cleanly. The co-precipitation literature on $NiFe_2O_4$, including the work referenced in the attachment, has repeatedly shown that annealing temperature controls the trade-off between phase purity and particle growth. Too little annealing preserves small size but weak crystallinity; too much annealing increases crystallinity but reduces the very nanoscale effects one may wish to study [35,39–41,43,48–51].

Representative synthesis-dependent microstructures are shown in Figure 4 to illustrate why nanoparticle morphology, agglomeration, porosity, and local nonuniformity must be considered when comparing wet-chemical and low-temperature preparation routes [39–43,49,50].

4.4. Hydrothermal/Solvothermal Synthesis and One-Dimensional Nanostructures

Hydrothermal and solvothermal methods are especially powerful because they give better control over crystal growth at moderate temperatures and can produce comparatively uniform particles, rods, or other anisotropic forms. The revised attachment rightly notes that hydrothermal routes are attractive when shape control and improved crystallinity are desired. Their disadvantages are the need for sealed autoclaves, elevated pressure, and slower processing. In nickel ferrite specifically, hydrothermal methods often reduce the defect density relative to mechanically milled powders while preserving small particle size, making them particularly useful for distinguishing true finite-size magnetic effects from milling-induced disorder. They also provide a route to one-dimensional

morphologies, which are especially important for separating shape anisotropy from pure size effects [36,39].

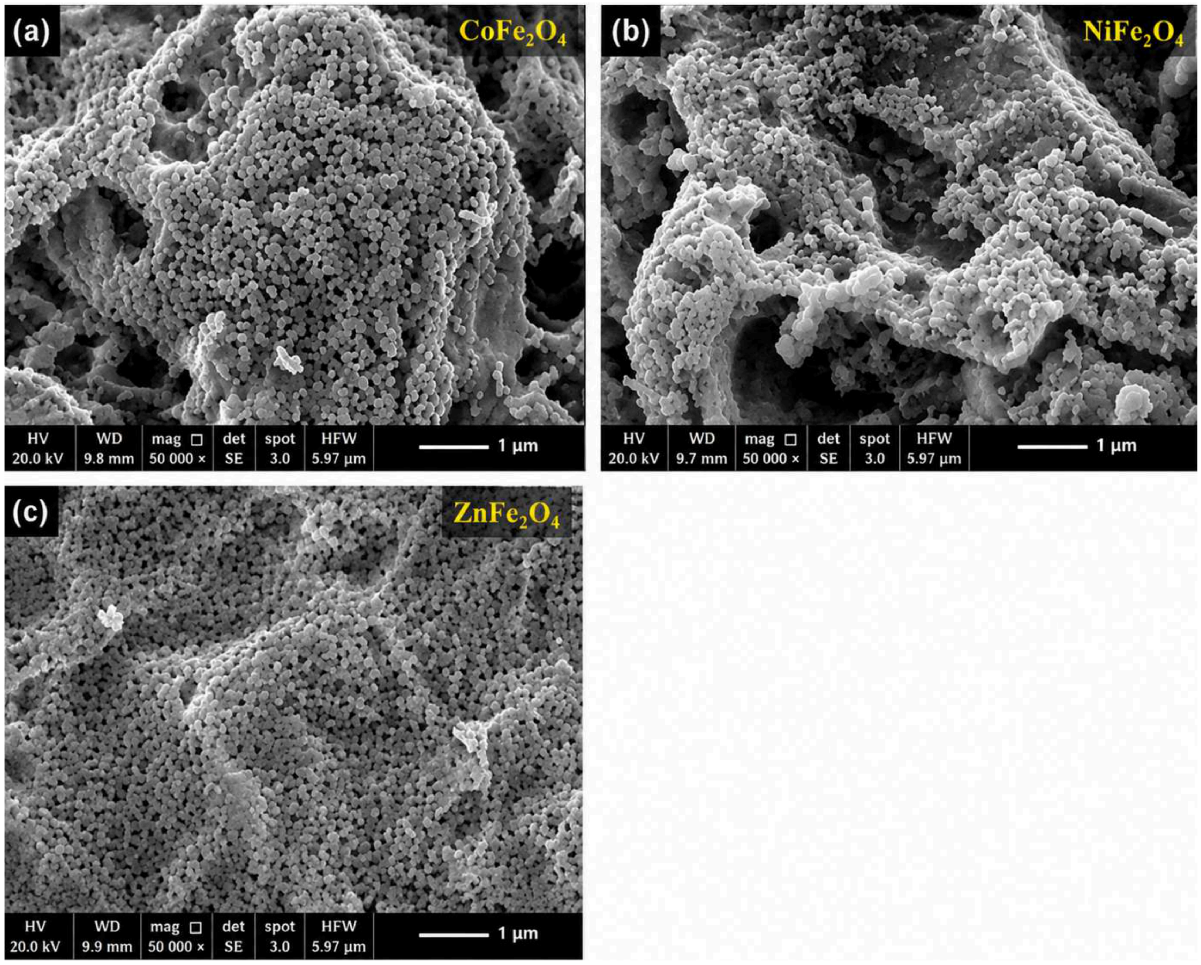


Figure 4. FESEM micrographs of spinel ferrite nanoparticles: (**a**) $CoFe_2O_4$, (**b**) $NiFe_2O_4$, and (**c**) $ZnFe_2O_4$, showing porous nanoparticle-based morphologies. $CoFe_2O_4$ and $ZnFe_2O_4$ exhibit clustered granular features, while $NiFe_2O_4$ shows a more cotton-like porous morphology. Reproduced/adapted from [41–50].

4.5. Sol–Gel and Combustion Approaches

Sol–gel synthesis occupies an intermediate position between molecular-level homogeneity and post-calcination crystallization. Because the metal ions are mixed on a fine chemical scale before gelation, sol–gel often yields highly homogeneous compositions and comparatively low-temperature formation of the spinel phase. The trade-off is that gel drying, burnout of organics, and calcination history strongly influence porosity, particle aggregation, and grain connectivity. The recent literature continues to regard sol–gel as one of the most versatile routes for nickel ferrite because it can generate powders suitable for both magnetic characterization and electrochemical applications. From a dimensionality perspective, sol–gel is attractive because it can occupy a broad middle ground: its product is smaller and more uniform than that produced in conventional ceramic synthesis, but often more crystalline and chemically homogeneous than aggressively milled powders. Combustion methods are faster and more energy-efficient but may produce fluffy, highly porous agglomerates whose local temperature history is difficult to control. As the attachment notes, the rapid exothermic reaction can form $NiFe_2O_4$ quickly, yet this speed often comes with broader particle-size distributions and local nonuniformity. Such materials

can be valuable for catalysis or adsorption, where surface area matters, but their magnetic interpretation must account for substantial microstructural heterogeneity [43–52].

4.6. Thin-Film Deposition Routes: Pulsed Laser Deposition and Sputtering

For thin films, the dimensionality-setting routes are pulsed laser deposition (PLD), radio-frequency sputtering, chemical spray or spin routes, and related vapor-phase approaches. PLD is particularly important in $NiFe_2O_4$ because it can transfer target stoichiometry efficiently and allows precise control over thickness. The attachments cite the thin-film PLD literature well, especially the work showing thickness-dependent grain size, coercivity, and saturation magnetization. PLD is also the route most closely associated with the ultrathin epitaxial $NiFe_2O_4$ literature, where off-equilibrium growth and cation redistribution are thought to play a major role. Its main disadvantages are cost, limited area scalability, and the sensitivity of ferrite films to oxygen pressure, substrate temperature, and post-annealing. Sputtering provides greater industrial relevance and good thickness control but frequently requires post-deposition annealing to develop high-quality ferrite order. The literature shows that ferrite films are highly sensitive to crystalline disorder, and that annealing often reduces the high saturation fields required by as-deposited disordered films [9,28–34,42].

The synthesis routes can therefore be arranged according to the kind of dimensionality problem they are best suited to reveal. Conventional ceramic synthesis is the route for bulk reference behavior. Ball milling and aggressive chemical precipitation are ideal for the finite-size and disorder regime. Hydrothermal and solvothermal methods are useful for small but better-ordered particles and one-dimensional structures. PLD and sputtering are the principal routes for thin films and ultrathin-film interface physics. This classification is more informative than listing methods alphabetically because it connects synthesis directly to magnetic interpretation. In practical terms, two nominally identical $NiFe_2O_4$ samples prepared by different routes should never be expected to have the same magnetic parameters unless their dimensionality, defect density, and cation distribution are also comparable [31,35,37,41–50].

The key practical implication is that synthesis route should be treated as a property-control variable. Ceramic synthesis provides bulk-like reference behavior, mechanochemical routes emphasize finite-size disorder, wet-chemical methods enhance surface functionality, hydrothermal/solvothermal routes improve shape control and crystallinity, and PLD/RF sputtering enable thickness- and interface-controlled film states. Therefore, meaningful comparison of $NiFe_2O_4$ properties requires the synthesis route, dimensionality, defect density, and cation-ordering state to be considered together.

5. Bulk Nickel Ferrite as the Equilibrium Reference State

Any dimensionality-based review must begin with a reference state, and for $NiFe_2O_4$ that state is the equilibrium or near-equilibrium bulk ferrite [51–56]. Bulk nickel ferrite is usually obtained through ceramic reaction and high-temperature sintering, conditions under which the spinel phase approaches equilibrium cation distribution and the relative influence of surfaces is minimized. A representative diffraction pattern of bulk-like $NiFe_2O_4$ is shown in Figure 5 to illustrate the cubic spinel reference structure discussed in this section. Bulk $NiFe_2O_4$ is therefore used here as the baseline against which nanoparticle magnetization suppression, one-dimensional shape-anisotropy effects, thin-film strain effects, and ultrathin-film interfacial enhancement are evaluated. This avoids treating each dimensional form as an isolated material and instead places all forms on a common structure–magnetism scale.

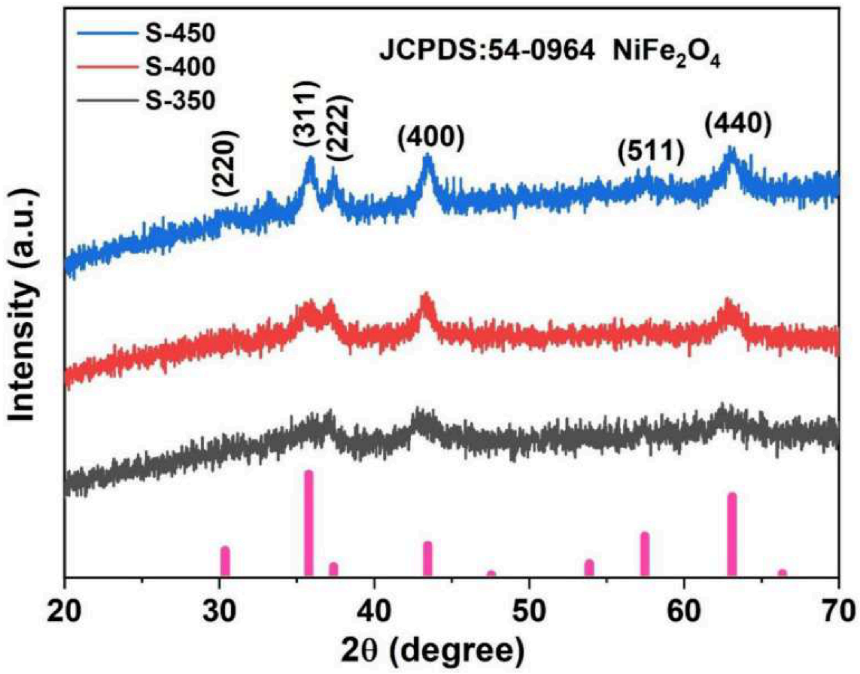


Figure 5. XRD patterns of $NiFe_2O_4$ samples annealed at 350 °C, 400 °C, and 450 °C, labelled as S-350, S-400, and S-450, respectively. The diffraction peaks at approximately 30.3°, 35.7°, 37.3°, 43.3°, 57.3°, and 63.0° correspond to the (220), (311), (222), (400), (511), and (440) planes of cubic spinel $NiFe_2O_4$, consistent with JCPDS No. 54-0964 [51–56].

From the viewpoint of magnetization reversal, bulk $NiFe_2O_4$ usually behaves as a multidomain ferrimagnet. Domain-wall motion therefore contributes significantly to reversal, keeping coercivity at moderate values. Grain size and porosity can alter the exact H_c measured experimentally, but the dominant physical point is that bulk specimens are not single-domain objects. This distinguishes them sharply from nanoparticles. It also means that the anisotropy landscape of bulk $NiFe_2O_4$ is averaged over many grains and domains rather than pinned primarily at surfaces or interfaces. Consequently, bulk measurements provide the clearest access to intrinsic spinel exchange and the least direct access to finite-size phenomena. Bulk $NiFe_2O_4$ also establishes the baseline temperature dependence. In the absence of strong finite-size or interface effects, the reduction in M_s with temperature is governed mainly by spin-wave excitations and standard ferrimagnetic thermal disordering. The Curie temperature remains high because the three-dimensional exchange network is fully connected. This is exactly why decreases in T_C reported for nanocrystalline samples are meaningful: they indicate not simply experimental scatter but a true weakening of long-range order caused by reduced coherence and increased surface or defect fractions. One may therefore summarize bulk $NiFe_2O_4$ with five characteristic features. First, it approaches the inverse-spinel limit more closely than nanoscale or ultrathin forms. Second, its magnetization is moderate but stable, making it a good reference for "normal" nickel ferrite behavior. Third, it is structurally coherent enough that the role of surface disorder is minimal. Fourth, its coercivity reflects multidomain reversal rather than blocking or superparamagnetism. Fifth, its Curie temperature is high and relatively insensitive to measurement details compared with nanopowders. These attributes justify using the bulk phase as the zero-order state in any dimensionality-based theory [2,6,7,17,19,57–60].

A representative room-temperature hysteresis loop for $NiFe_2O_4$ is presented in Figure 6 to illustrate the moderate ferrimagnetic response and the role of the bulk phase as the magnetic reference state.

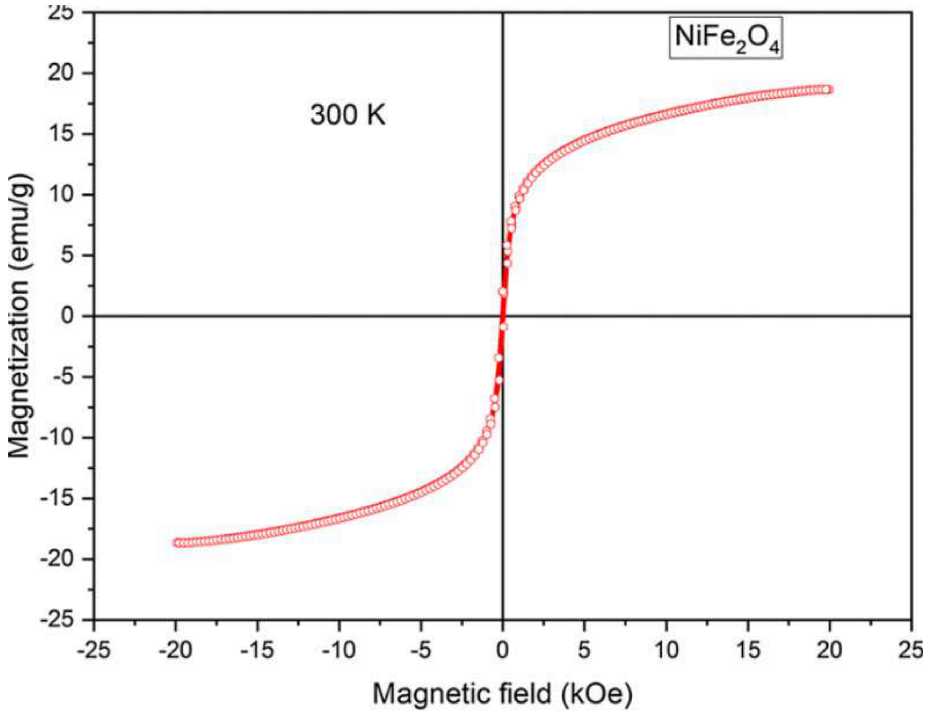


Figure 6. Room-temperature magnetic hysteresis loop of $NiFe_2O_4$ measured at 300 K, showing ferrimagnetic behavior with nonlinear magnetization response under an applied magnetic field of ±20 kOe [57–60].

The importance of the bulk reference becomes most obvious when one examines claims of enhanced or suppressed magnetization in reduced-dimensional samples. Without a clear baseline, one might misinterpret a nanoparticle magnetization of 24 emu g^{-1} as simply "normal" or a thin-film value above 250 emu cm^{-3} as automatically superior. In reality, both numbers have meaning only relative to the bulk reference and to the defect and inversion terms that dimensionality introduces. Thus, the bulk state does not merely occupy the first section of a review; it anchors the entire interpretive framework. In practical materials design, bulk nickel ferrite remains relevant whenever thermal robustness, modest coercivity, and high-frequency resistive performance are needed without the complications of nanoscale disorder or interfacial strain. Yet scientifically, its greater value lies in being the cleanest expression of the intrinsic ferrimagnetic spinel before dimensionality begins to rewrite the magnetic script. The sections that follow can therefore be read as systematic departures from this equilibrium reference [24,28–30,57–61].

6. Nanoparticles and Nanocrystalline $NiFe_2O_4$: Finite-Size Suppression, Spin Canting, and Blocking

The attachment-based dataset also contains representative experimental evidence for the nanoparticle regime. Figure 7 below summarize the characteristic reduction in spontaneous magnetization under strong milling and the size-dependent blocking/coercivity behavior that marks the transition from superparamagnetic to blocked single-domain states [6,7,61].

The nanocrystalline regime is where dimensionality first becomes impossible to ignore. Once the characteristic diameter of $NiFe_2O_4$ is reduced to a few tens of nanometers or below, the ratio of surface atoms to interior atoms increases rapidly, and the magnetic response begins to depart from the bulk state in a qualitatively new way. The uploaded attachment based on the work of Nabiyouni and co-workers captures this transition well: increasing milling time reduces the grain size and leads simultaneously to lower saturation

magnetization and a lower Curie temperature. This is one of the clearest illustrations of the finite-size problem in nickel ferrite. The essential reason for this suppression is surface spin disorder. In a bulk inverse spinel, most cations are fully coordinated and participate in well-defined superexchange pathways. Near the surface of a nanoparticle, however, oxygen coordination is incomplete, bond angles are perturbed, and local symmetry is reduced. The result is that surface moments no longer align collinearly with the core in the same way: some spins cannot; others become weakly coupled or even frustrated [15,16,24,37,38,61].

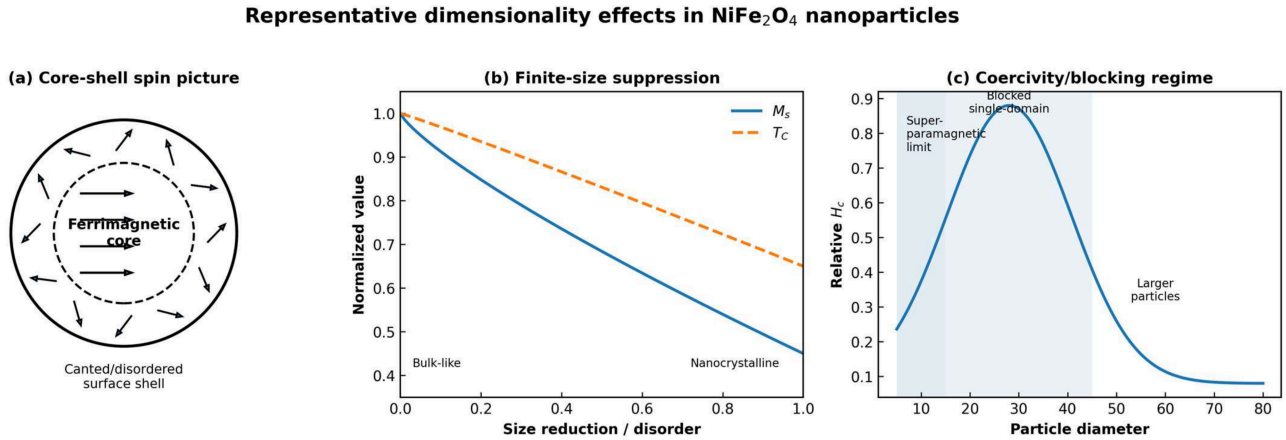


Figure 7. Author-prepared schematic summarizing the representative nanoparticle mechanisms in $NiFe_2O_4$: (**a**) ferrimagnetic core with a canted/disordered surface shell; (**b**) finite-size/disorder-induced suppression of saturation magnetization and Curie temperature; and (**c**) non-monotonic coercivity associated with the transition between superparamagnetic, blocked single-domain, and larger-particle regimes [6,7,24,26,61].

The effective nanoparticle may therefore be pictured as a ferrimagnetic core surrounded by a magnetically disordered shell. Equation (3) introduced earlier formalizes this by assigning a disordered shell thickness δ that subtracts from the bulk-like magnetic volume. The smaller the particle, the larger the relative contribution of that shell, and the lower the measured M_s. This interpretation also explains why the suppression of magnetization is often accompanied by unsaturated M(H) behavior at high fields. A canted or frustrated surface shell cannot be aligned as easily as a uniform ferrimagnetic core. Consequently, the magnetization curve may continue to rise at fields well above those needed to saturate the core. The same logic appears in the older ferrite nanoparticle literature more broadly and is consistent with the mechanosynthesized $NiFe_2O_4$ studies cited in the web search results. In practical terms, a reduced M_s in a nanoparticle sample should not be interpreted simply as "worse ferrite." It is often the fingerprint of a core–shell-like magnetic architecture imposed by dimensionality. Curie temperature suppression in nanocrystalline nickel ferrite follows from the same picture. The ordering temperature is governed by the average exchange energy that stabilizes the ferrimagnetic state. If a significant fraction of the material consists of weakly coupled or frustrated spins, the effective exchange field decreases and the long-range order collapses at a lower temperature [15,16,24,55,56].

The decrease from about 570 °C in bulk to about 517 °C in nanocrystalline $NiFe_2O_4$ reported in the attachment is therefore physically reasonable and theoretically important. It confirms that nanoscale dimensionality does not merely affect low-temperature anisotropy or room-temperature coercivity; it changes the thermodynamic stability of the ferrimagnetic state itself. The size dependence of coercivity adds further richness. Unlike magnetization, coercivity is usually non-monotonic with particle size. In large particles or bulk grains, reversal occurs in part by domain-wall motion, which keeps H_c moderate. As the particles become smaller and approach the single-domain size, domain-wall formation

becomes energetically expensive and reversal shifts toward coherent or quasi-coherent rotation, so coercivity rises. But once the particles become so small that K_{eff} V is comparable to thermal energy, the magnetization direction fluctuates on experimental time scales and H_c falls toward zero. This produces the classical coercivity maximum at an intermediate size. The attachment's discussion of nearly zero remanence and coercivity for a nanocrystalline sample is fully consistent with the system having moved into or near the superparamagnetic regime [15–18,37,38,61].

Nanoparticles' synthesis route matters enormously here because the same nominal size may have very different defect populations depending on whether it was achieved by milling, co-precipitation, hydrothermal growth, or combustion. Ball-milled nanoparticles often contain high internal strain and defect-rich surfaces, which amplify suppression of magnetization. Chemically grown nanoparticles may be more crystalline at similar size and therefore show larger M_s. This is why comparisons of magnetization values across the $NiFe_2O_4$ nanoparticle literature often show significant scatter even at similar reported sizes. A purely size-based plot therefore misses an important truth: finite size and structural disorder enter simultaneously, and they are not easily separable unless the synthesis route is controlled. There is also a dimensionality crossover hidden inside the nanoparticle regime itself. At diameters of several tens of nanometers, the particles may still be ferrimagnetically blocked at room temperature and exhibit measurable coercivity. As the size decreases further, room-temperature superparamagnetism emerges, though the same particles may remain blocked at lower temperature. Thus, the dimensionality problem is not solved simply by calling all nanopowders "nanoscale." One must specify whether the particles are multidomain, single-domain blocked, or effectively superparamagnetic under the measurement conditions [35–41,43,48–54].

One-dimensional nanostructures such as nanofibers, nanotubes, and rods belong partly to the nanoparticle regime but deserve separate attention because shape anisotropy begins to compete with surface disorder. Several internet reports on $NiFe_2O_4$ nanofibers show that coercivity and anisotropy can be stabilized relative to roughly isotropic nanoparticles because the elongated geometry provides an additional preferential magnetization axis. This is a reminder that dimensionality is not equivalent to particle diameter alone. Morphology matters. A 20 nm spherical particle and a 20 nm diameter, 500 nm long fiber have very different magnetic-energy landscapes even if both are nanoscale in one dimension. From an applications standpoint, the nanoparticle regime is both the most promising and the most delicate. It is promising because superparamagnetic or weakly blocked $NiFe_2O_4$ nanoparticles can be manipulated by external fields, dispersed in fluids, and used for magnetic hyperthermia, separation, catalysis, adsorption, or battery electrodes. It is delicate because the same surface-driven physics that enables these uses also undermines saturation magnetization and complicates reproducibility [27,36,39].

A successful nanoparticle design therefore requires balancing high surface area with sufficient core ordering. The dimensionality-based theory developed in this review suggests that this balance can be approached by maximizing crystallinity and controlling cation distribution while accepting that some surface-driven suppression of M_s is unavoidable. The major theoretical lesson of the nanoparticle regime is therefore this: dimensional reduction from bulk to nanoparticles does not simply scale down the same ferrimagnet. It creates a two-component magnetic entity composed of a bulk-like ferrimagnetic core and a non-bulk surface shell. The experimentally measured magnetization, coercivity, and Curie temperature are all averages over that heterogeneous entity. This insight is one of the key foundations for understanding why $NiFe_2O_4$ behaves so differently across dimensions [15,16,25,26,35–41].

7. One-Dimensional Nanostructures and Anisotropy Engineering

One-dimensional nickel ferrite nanostructures, including nanofibers, nanorods, nanotubes, and chain-like assemblies, occupy an intermediate conceptual space between isotropic nanoparticles and continuous thin films. They are nanoscale in diameter, so they inherit strong surface effects, yet they are extended along one axis, so shape anisotropy becomes a first-order factor. This regime is especially instructive because it demonstrates that dimensionality affects not only the fraction of surface spins but also the geometry of the anisotropy landscape. Figure 8 provides a processed schematic representation of this concept and shows how the elongated geometry introduces a preferred magnetic axis while surface disorder remains important at the nanoscale diameter [27,36,39]. The key distinction between isotropic nanoparticles and one-dimensional $NiFe_2O_4$ nanostructures is that the latter introduce a preferred magnetic axis through their elongated geometry. One-dimensional $NiFe_2O_4$ nanostructures such as nanofibers, nanorods, nanotubes, and chain-like assemblies belong partly to the nanoparticle regime but require separate treatment because shape anisotropy competes with surface disorder. The literature on electrospun $NiFe_2O_4$ nanofibers, $NiFe_2O_4$ nanorods, $NiFe_2O_4$ nanotubes/nanowires, and general magnetic nanowire systems shows that elongated morphology can introduce a preferential magnetization axis along the long direction and can modify coercivity, remanence, and reversal behavior compared with nearly isotropic nanoparticles of similar diameter. Therefore, dimensionality is not equivalent to particle diameter alone. For example, a nearly spherical 20 nm $NiFe_2O_4$ particle and a 20 nm diameter, 500 nm long $NiFe_2O_4$ fiber/rod have different demagnetizing factors, aspect ratios, shape-anisotropy energies, and magnetic reversal barriers, even though both contain at least one nanoscale dimension. This morphology-dependent magnetic response is consistent with reported studies on $NiFe_2O_4$ nanofibers and nanorods and with the broader nanomagnetism literature on shape anisotropy in elongated magnetic nanostructures. In nanofibers, nanorods, nanotubes, and chain-like assemblies, the demagnetizing field is minimized when magnetization aligns along the long axis. This shape anisotropy can increase the effective energy barrier for reversal and can partially delay the onset of superparamagnetic relaxation compared with spherical nanoparticles of similar diameter, provided that intergrain exchange continuity is not destroyed by porosity or weakly connected grains.

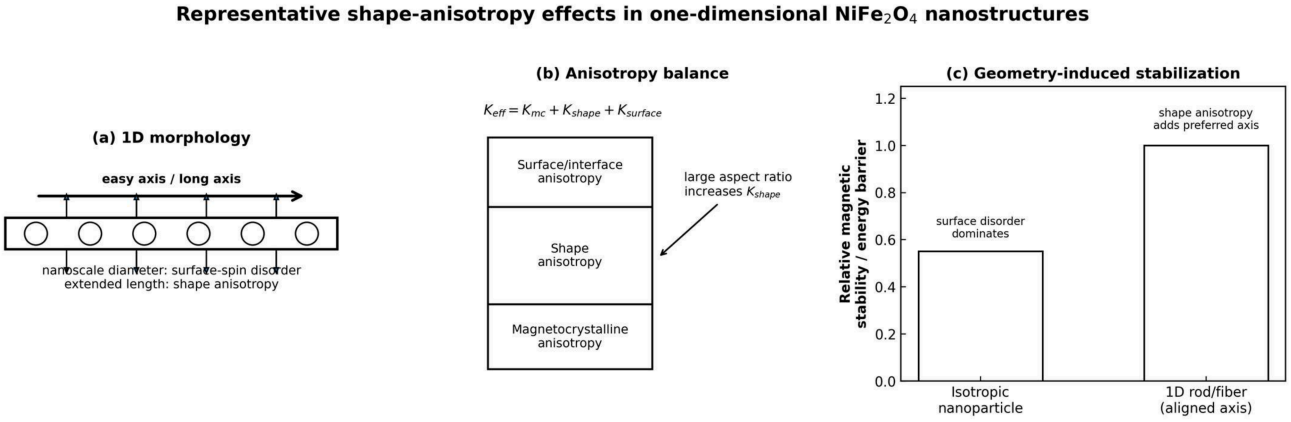


Figure 8. Schematic illustration of the magnetic role of one-dimensional $NiFe_2O_4$ nanostructures. The elongated rod/fiber geometry introduces a preferred magnetization direction along the long axis, while the nanoscale diameter preserves a significant surface-disordered contribution. The effective anisotropy is governed by coupled magnetocrystalline, shape, and surface/interface terms, with the shape contribution enhancing magnetic stability relative to isotropic nanoparticles of comparable diameter [6,7,24,26,62].

In a one-dimensional magnetic object, the demagnetizing field is minimized when the magnetization lies along the long axis. As a result, even when the constituent material is magnetically soft in bulk form, the morphology itself can create a preferred direction and stabilize remanence or coercivity relative to isotropic particles. For $NiFe_2O_4$ this is important because the moderate intrinsic anisotropy of the spinel can be significantly reshaped by geometry. The total anisotropy therefore becomes a sum of magnetocrystalline, shape, and surface contributions, and shape anisotropy may dominate if the aspect ratio is sufficiently large. This is one reason why nickel ferrite nanofibers and rods often exhibit coercivities and loop shapes different from those of nanoparticles of similar diameter [17,19,27,36].

The literature on one-dimensional $NiFe_2O_4$ is smaller than the literature on nanopowders or thin films, but it is scientifically revealing. Electrospun or template-derived nanofibers commonly show elongated grains linked along the fiber axis. Such structures can preserve partial exchange continuity along the long direction even while suffering surface disorder radially. The magnetic consequence is a competition between a favorable axis of magnetization and a radially disordered shell. If the internal coherence is good enough, the nanofiber may retain appreciable remanence and coercivity at room temperature despite a nanoscale diameter. If, however, the fiber is composed of weakly coupled nanograins with large intergranular disorder, the benefit of shape anisotropy will be partly lost. This regime is theoretically useful because it separates two factors that are often confounded in ordinary nanoparticles: volume and geometry. A one-dimensional $NiFe_2O_4$ nanostructure can have a small diameter and therefore a large surface fraction, yet the elongated shape can delay the onset of fully superparamagnetic behavior by increasing the effective energy barrier for reversal. In terms of Equation (4), the anisotropy constant K_{eff} is no longer controlled only by crystal-field effects and surface disorder; it receives a substantial shape contribution. Thus, one-dimensional dimensionality demonstrates that finite size does not always mean lower coercivity. Depending on aspect ratio and microstructural connectivity, nanoscale objects may become magnetically more stable along a preferred axis than similarly sized isotropic particles [27,36,39].

The synthesis route is again crucial. Hydrothermal and electrospinning methods are especially attractive for one-dimensional $NiFe_2O_4$ because they allow aspect ratio control without the intense mechanical damage associated with milling. Template-based methods can create nanotubes or porous wires, though porosity introduces additional surface disorder. From the viewpoint of applications, one-dimensional nickel ferrite is promising for aligned absorber structures, anisotropic sensors, and magnetic field-guided assemblies. Yet the literature still lacks a fully unified theory comparing rods, fibers, and tubes on equal footing. Most studies remain synthesis-specific. From a review perspective, the main reason to include one-dimensional $NiFe_2O_4$ is that it broadens the concept of dimensionality beyond simple particle diameter or film thickness. Shape itself is a dimensionality variable. Once this is acknowledged, the behavior of $NiFe_2O_4$ can be organized more systematically: isotropic nanoparticles emphasize surface disorder; one-dimensional nanostructures emphasize surface disorder plus shape anisotropy; thin films emphasize strain and interfaces; and ultrathin films emphasize all of these together with nonequilibrium cation redistribution. This hierarchical view is one of the strengths of the present review [36,39].

8. Thin Films: Thickness, Strain, Anti-Phase Boundaries, and Anisotropy

For the thin-film regime, the uploaded attachment is especially useful because it collects multiple classic datasets on thickness-driven changes in crystallinity, coercivity, and saturation magnetization. Figure 9a–d visually support the argument that film thickness influences $NiFe_2O_4$ simultaneously through grain size, texture, anti-phase boundaries, and defect relaxation. For the thin-film regime, the uploaded attachment is especially useful

because it collects multiple classic datasets on thickness-driven changes in crystallinity, coercivity, and saturation magnetization [5,20,21,63–66]. These figures visually support the argument that film thickness influences $NiFe_2O_4$ simultaneously through grain.

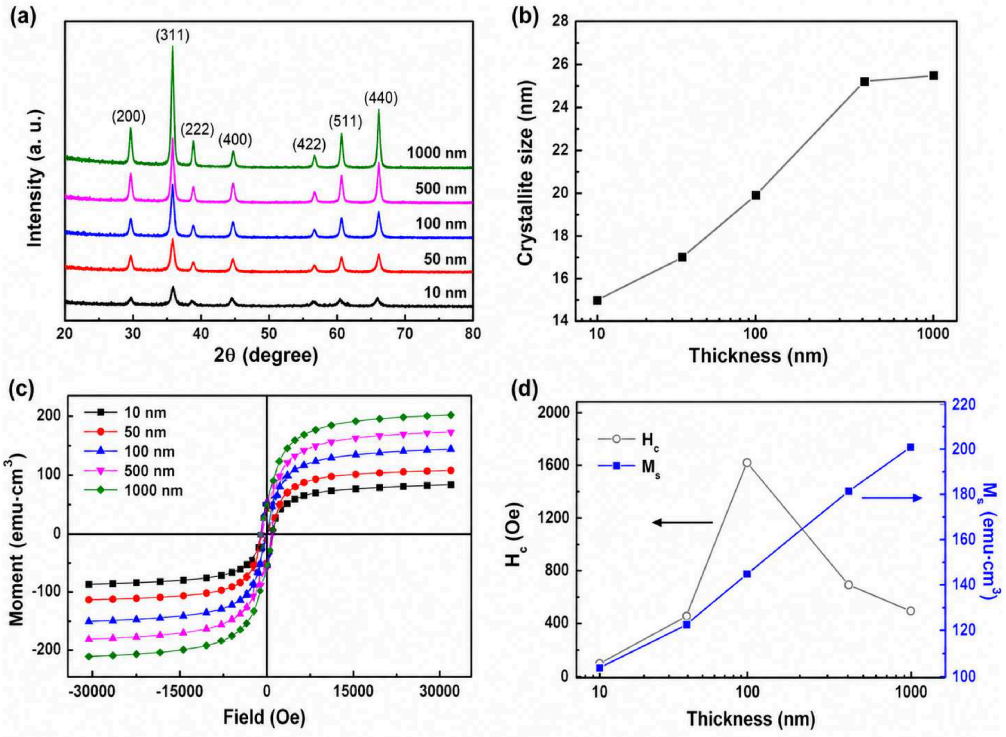


Figure 9. Thickness-dependent structural and magnetic properties of spinel ferrite thin films. (**a**) XRD patterns show enhanced spinel crystallinity with increasing thickness. (**b**) Crystallite size increases from ~15 to ~25 nm. (**c**) Hysteresis loops reveal thickness-enhanced magnetic moment. (**d**) M_s increases monotonically, while H_c peaks at intermediate thickness, reflecting competing effects of grain growth, anisotropy, strain relaxation, and domain evolution [5,20,21,63–66].

Thin-film nickel ferrite is where dimensionality becomes technologically and conceptually richest. A film is not merely a flattened bulk specimen. It is a mechanically clamped magnetic oxide grown under nonequilibrium conditions, strongly influenced by substrate mismatch, oxygen stoichiometry, deposition kinetics, and post-annealing. As a consequence, the properties of $NiFe_2O_4$ films often vary strongly with thickness, even when composition is nominally constant. This theme runs throughout the papers summarized in the uploaded attachments and remains central in the internet literature as well [9,28–34,42].

The PLD study provides a useful benchmark for thickness-driven microstructural and magnetic evolution in nickel ferrite films.. In that work, nickel ferrite films of thickness roughly 62–176 nm showed increasing grain size with increasing thickness, while coercivity decreased as the films became thicker. The interpretation proposed there that thinner films possess more grain boundaries or defect pinning centers, and therefore larger coercivity is physically plausible and consistent with Equation (7). At smaller thickness, the film has had less opportunity to coarsen and relax, so both grain-boundary pinning and defect-mediated anisotropy are stronger. As the thickness increases, grains become larger and the density of obstructive boundaries decreases, reducing H_c. This is a classic dimensionality effect in oxide films and should be regarded as a robust trend rather than an idiosyncratic experimental detail. At the same time, thickness does not control only grain size. It also controls the degree of strain relaxation. A very thin film often remains highly strained because it conforms more closely to the substrate lattice. As thickness increases, misfit may be relieved through defects, dislocations, or a gradual return toward the bulk lattice

parameter. Since $NiFe_2O_4$ is magnetoelastic, that strain state feeds directly into anisotropy. The net result is that saturation magnetization and coercivity need not vary monotonically with thickness in the same way. A thickness that maximizes grain growth may not maximize magnetization if the same thickness also favors anti-phase boundaries or partial phase separation. This helps explain why some film series show non-monotonic M_s versus thickness even when H_c shows a clearer trend. Anti-phase boundaries (APBs) deserves special emphasis. In spinel ferrite films grown on substrates, APBs form when adjacent islands nucleate with a relative translational offset and then coalesce [31–34,42].

Across such a boundary, the cation network is out of registry, so exchange coupling can become frustrated or antiferromagnetically unfavorable. The practical magnetic consequence is that the film may require very high fields to approach saturation because spins across APBs are not easily aligned. This problem is especially important in ferrites grown epitaxially or semi-epitaxially on lattice-mismatched substrates. Even when the XRD pattern appears phase-pure, APBs can reduce the effective magnetization and alter loop shape dramatically. The older ferrite thin-film literature and the Caltun paper both underscore how sensitive ferrite films are to crystalline disorder and how annealing improves magnetic behavior by improving structural order. Texture and orientation are additional thin-film variables. In some growth conditions, $NiFe_2O_4$ films exhibit strong (400) or related texture, whereas under others they remain polycrystalline or even amorphous as deposited. Texture matters because magnetocrystalline anisotropy is orientation dependent. A textured film can therefore exhibit different in-plane and out-of-plane reversal behavior than an unoriented polycrystalline film. The attachment summarizing O.F. Caltun's PLD work, for example, points to the emergence of textured structures after annealing and the associated change from paramagnetic-like behavior in the as-deposited amorphous state to ferrimagnetic loops in the annealed state. The film problem also demonstrates the importance of stoichiometry and oxygen control. Ferrite films grown at low oxygen pressure may contain Fe-rich secondary phases or oxygen-deficient regions, both of which alter the magnetic response. Because ferrites are transition-metal oxides, oxygen vacancies affect both cation valence balance and exchange pathways [9,28–34,42].

In practical terms, thin-film synthesis of $NiFe_2O_4$ is a multi-parameter optimization problem involving thickness, substrate, oxygen pressure, deposition temperature, and post-anneal. This complexity explains why the reported saturation magnetization values for nominally similar films vary widely across the literature. The web literature provides important support for this interpretation. Recent reports on $NiFe_2O_4$ thin films stress the role of strain in determining anisotropy and magnetic response, and some explicitly identify film strain as the dominant factor in anisotropy control [26,29,67–70]. This confirms that thickness in $NiFe_2O_4$ films should never be discussed without strain. Thickness affects grain size, grain boundaries, and APBs, but it also changes how much of the epitaxial or pseudomorphic strain is retained. Therefore, a genuinely dimensionality-based account of $NiFe_2O_4$ thin films must treat thickness and strain as inseparable variables. From a broader theoretical viewpoint, thin films reveal why dimensionality cannot be reduced to particle surface fraction alone. In a nanoparticle, the main non-bulk term is surface spin disorder. In a film, the free surface matters, but the substrate interface and the defect network inside the film are equally important. The microstructural coherence function introduced earlier is thus especially useful here because it can be low even in a crystalline-looking film if APBs are abundant. This is precisely why film magnetization values cannot be interpreted from XRD peak width alone. Technologically, the thin-film regime is central for microwave devices, integrated ferrite components, spin filters, and oxide heterostructures. Scientifically, it is central because it exposes the interplay of all three functions proposed in this review: cation distribution, coherence, and surface/interface order. It is therefore the

natural bridge between nanoparticle finite-size physics and the ultrathin-film anomalies discussed next [34,49,50,70–75].

9. Ultrathin Epitaxial Films: Giant Magnetization, Nonequilibrium Inversion, and Controversy

The ultrathin-film limit is the most controversial region of the dimensionality landscape because enhanced magnetization can emerge together with substrate- and interface-sensitive behavior, as shown in Figure 10 [9,76].

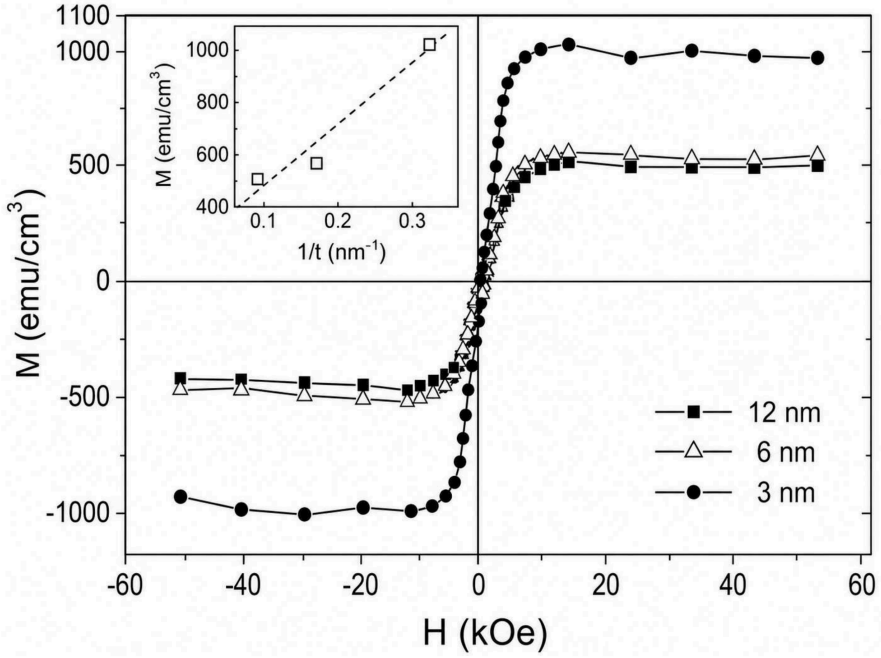


Figure 10. Representative hysteresis comparison for ultrathin $NiFe_2O_4$ films reproduced from the uploaded attachment [9,76]. The inset shows the approximate linear dependence of magnetization on inverse thickness $1/t$, indicating a strong finite-size and surface/interface contribution to the magnetic behavior.

The attachment reproduces a representative ultrathin-film hysteresis comparison that complements the APS literature discussed in this section.

The most controversial and conceptually provocative regime in the entire nickel ferrite literature is the ultrathin epitaxial regime. Here the thickness is not merely below 100 nm but is only a few nanometers, sometimes corresponding to only a few tens of unit cells. Under such conditions, $NiFe_2O_4$ can no longer be viewed as a slightly perturbed bulk ferrite. The entire film is effectively an interface-dominated material. It is in this regime that Lüders and co-workers reported enhanced magnetic moment and even conductive behavior in ultrathin epitaxial $NiFe_2O_4$ films grown on $SrTiO_3$, with magnetization values roughly 250% larger than those of the bulk. This result attracted substantial attention because it seemed to violate the usual finite-size expectation that reducing thickness should suppress, not enhance, the magnetic moment. The explanation proposed in that work invoked an anomalous distribution of Ni and Fe cations over tetrahedral and octahedral sites induced by off-equilibrium growth conditions and interface effects. In the language of the present review, the inversion-related correction term $\Delta M_{\mathrm{inv}}(t)$ in Equation (6) becomes strongly positive and outweighs the normally negative surface and defect terms. If true, this means that ultrathin-film dimensionality can fundamentally re-engineer the ferrimagnetic balance of $NiFe_2O_4$ by altering which ions occupy which sublattice. The significance of this claim goes beyond $NiFe_2O_4$ itself [28–30].

It implies that an oxide spinel can be transformed into a new magnetic state by epitaxial stabilization rather than by chemical doping. Such a possibility is of enormous interest for spintronic heterostructures, where an insulating ferrimagnet with tunable moment and perhaps spin-filter functionality could be extremely valuable. This is one reason why the ultrathin $NiFe_2O_4$ problem remains highly cited and widely discussed. At the same time, the subsequent literature has shown that the situation is subtler than a simple "giant moment" narrative. Later studies of ultrathin epitaxial $NiFe_2O_4$ and related ferrites pointed out that substrate artifacts, parasitic paramagnetic signals, strain state, and the exact oxygen environment during growth can all complicate the interpretation of magnetometry data. Some work indicated that the cation distribution remained more homogeneous than initially suspected, while other work emphasized the importance of subtracting spurious substrate contributions carefully. The 2020 literature on enhanced magnetization in ultrathin $NiFe_2O_4$ films, for example, revisited the cation-distribution question using more advanced spectroscopic tools and reinforced the need for caution when attributing large moments solely to inversion changes. From the standpoint of this review, the value of the ultrathin-film literature is not that it conclusively proves one mechanism. Its value is that it demonstrates how powerful dimensionality can become once the film thickness is reduced to the scale of the interface itself. In ordinary thin films, APBs, strain, and grain structure dominate. In ultrathin epitaxial films, nonequilibrium site occupancy and electronic reconstruction can become equally important. The film is effectively all interface, and that means its magnetic state can no longer be inferred from bulk crystal chemistry alone. The ultrathin regime therefore forces a refinement of the dimensionality framework. Surface/interface spin order is no longer just a reduction term; it can become a reconstruction term. Similarly, the cation-distribution function is no longer a small perturbation away from the inverse-spinel value; it may become a major driver of the moment. Microstructural coherence remains important, but the defects that matter are now those associated with epitaxial registry, step structure, and buried interfacial disorder rather than simply grain boundaries in a polycrystalline film. A useful way to organize the ultrathin-film controversy is to ask which terms in Equation (6) dominate. If $\Delta M_{\mathrm{interface}}(t)$ and $\Delta M_{\mathrm{strain}}(t)$ are negative and large, the magnetization should fall below the bulk value, as intuition suggests. If $\Delta M_{\mathrm{inv}}(t)$ becomes positive and even larger under nonequilibrium growth, the net moment may exceed the bulk value. If the measured enhancement arises instead from incomplete subtraction of substrate or parasitic signals, then the intrinsic film moment may have been overestimated [28–30].

These scenarios are experimentally distinguishable in principle, but only with a combination of magnetometry, x-ray absorption, XMCD, spectroscopy, and careful structural analysis. This explains why ultrathin $NiFe_2O_4$ remains a live problem rather than a settled one. What seems robust, however, is that ultrathin $NiFe_2O_4$ is not simply a thinner version of ordinary thin films. It occupies its own dimensionality regime. The most important lesson is therefore not the exact percentage enhancement reported in any one study, but the fact that dimensionality reduction to a few nanometers can qualitatively transform the spinel magnetic state. For a review focused on dimensionality, this is a crucial conclusion and one of the clearest demonstrations that $NiFe_2O_4$ can exhibit non-intuitive physics when pushed far from the bulk scale [28–30].

10. Dimensionality Property Map: Bulk, Particles, Films, and Ultrathin Limits

At this stage, it is useful to compress the preceding sections into a single dimensionality property map. The most stable point in the map is bulk $NiFe_2O_4$. Here the inverse-spinel state is near equilibrium, the exchange network is three-dimensional and coherent, domain-

wall motion contributes to reversal, and the magnetic properties cluster around the familiar reference values. Surface disorder is negligible, APBs are absent in the thin-film sense, and cation redistribution is largely controlled by thermodynamics rather than by growth kinetics. Reducing the characteristic dimension into the nanocrystalline particle regime shifts the balance toward free surfaces. Surface spin canting and frustration become dominant negative corrections to the moment. Coercivity first rises toward the single-domain window and then falls as thermal fluctuations become strong enough to induce superparamagnetic relaxation. Curie temperature decreases because exchange connectivity is effectively diluted by disordered surface regions. In this regime, the most important experimental variables are particle size, crystallinity, and synthesis-induced defect density. Changing the geometry from isotropic particles to one-dimensional structures introduces a new anisotropy axis. Surface effects remain significant because the diameter is nanoscale, but shape anisotropy can stabilize the magnetic state relative to spherical nanoparticles. Consequently, nanofibers and rods may show coercivity and remanence not predictable from size alone [15–18,24–34,42].

This regime is defined by the competition between a negative surface-disorder term and a positive shape-anisotropy term. Moving to ordinary thin films replaces free-surface control with interface and defect-network control. Thickness determines grain size, relaxation, and texture, while the substrate introduces strain and often anti-phase boundaries. Magnetization is no longer governed simply by surface shell fraction; it depends on how coherent the exchange network remains through the film plane and across planar defects. Coercivity may increase as thickness decreases because defect density and pinning rise, but magnetization may vary non-monotonically depending on phase purity and APB density. Finally, the ultrathin epitaxial regime makes the interface itself the controlling unit of dimensionality. At only a few nanometers, every cation is close to a surface or interface, and nonequilibrium cation redistribution can become a first-order effect. If the inversion degree changes significantly, the net ferrimagnetic moment can deviate strongly possibly even upward from the bulk reference. This is the regime in which dimensionality ceases to be a small perturbation and becomes a route to an emergent magnetic state. This map leads to a practical classification of the dominant mechanisms in each regime. Bulk: Equilibrium inversion and three-dimensional superexchange. Nanoparticles: Surface spin disorder and blocking physics. One-dimensional nanostructures: Surface disorder plus shape anisotropy [15–18,28–34,42].

Thin films: strain, APBs, and thickness-controlled microstructural coherence. Ultrathin epitaxial films: interface-driven inversion changes, reconstruction, and strong substrate coupling. Although these categories overlap, they provide a useful organizing principle for the literature and help explain why reports from different dimensional regimes cannot be compared casually. The map also clarifies why synthesis method and dimensionality cannot be separated. Ceramic reaction naturally populates the bulk regime. Milling drives the material toward the disorder-rich nanoparticle regime. Hydrothermal and solvothermal methods can access better-ordered nanoparticles and one-dimensional forms. PLD and sputtering define the thin-film and ultrathin regimes. Thus, dimensionality in $NiFe_2O_4$ is not an abstract geometric descriptor; it is the physical consequence of how the material is made and stabilized. A review article should ideally end not with a list of observations but with a conceptual simplification. In the present case, the simplification is that all reported magnetic behavior in $NiFe_2O_4$ can be interpreted as competition between bulk ferrimagnetic order and dimensionality-specific perturbations. The nature of those perturbations changes systematically with dimensionality. This is the deepest unifying message that emerges from combining your attachments with the broader journal literature [15–18,28–34,42].

11. Structure-Morphology-Magnetism Correlation from Microscopy, Diffraction, and Magnetic Measurements

The discussion below is written as a practical reading of the datasets rather than a caption-only archive, with emphasis on what each image set proves structurally and magnetically and why that matters for $NiFe_2O_4$ dimensionality control [5–7,20–26,77–83].

Practically, the SEM plate associated with Figure 11 shows that mechanochemical refinement does not generate isolated uniform nanocrystals; it produces dense agglomerates built from much finer subunits. This means that the measured magnetization is controlled simultaneously by crystallite refinement and by magnetic interaction within agglomerates, which explains the incomplete saturation and the strong milling-time sensitivity reported for mechanosynthesized $NiFe_2O_4$ [7,84].

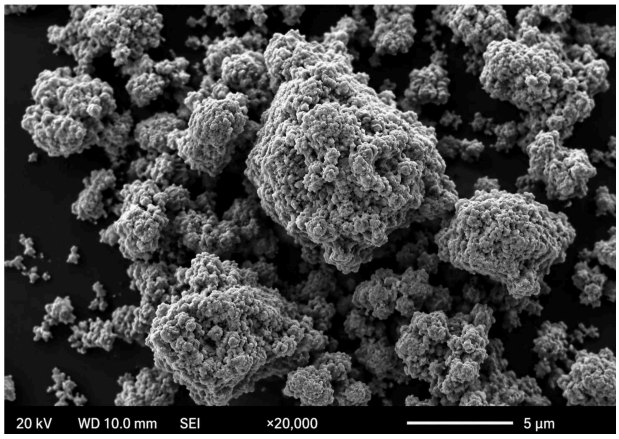


Figure 11. Mechanochemical milling: SEM micrographs of nickel ferrite powders after 16 h milling, showing agglomerated nanometric particles embedded within larger micrometric clusters [7,84].

The Figure 11 set linked to Figure 12 should be read as direct structural evidence that film thickness in PLD-grown $NiFe_2O_4$ is an active growth variable rather than a passive geometric parameter. As deposition time increases, the spinel reflections become more pronounced, whereas iron-oxide impurity peaks can still appear in selected films. Practically, this means that thicker films are magnetically useful only when phase purity improves at the same time [5]. Figure 12 shows pulsed laser deposited $NiFe_2O_4$ thin films: XRD patterns for the target and films deposited for different durations, highlighting thickness-linked crystallization and secondary-phase sensitivity [5,85].

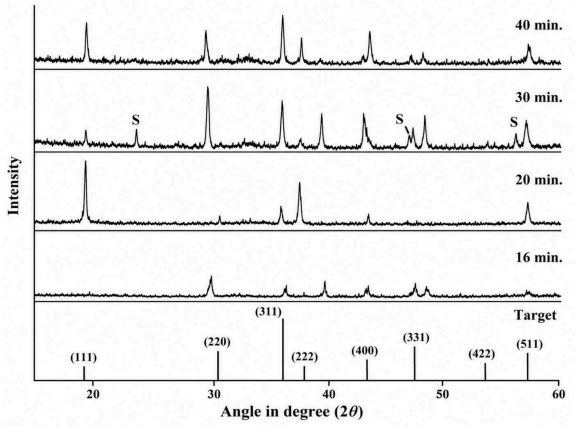


Figure 12. Pulsed laser deposited $NiFe_2O_4$ thin films: XRD patterns for the target and films deposited for different durations, highlighting thickness-linked crystallization and secondary-phase sensitivity [5,85].

Figure 13 brings morphology, vibrational structure, and magnetism into one experimental chain. The AFM panels show thickness-driven coarsening of the granular surface, the Raman response reflects thickness-sensitive changes in octahedral and tetrahedral-site environments, and the M-H curves show a stronger ferrimagnetic state as the film approaches the thicker end of the series. In practice, the thickness effect is therefore a combined grain-size, cation-site, and exchange-continuity effect [5,86].

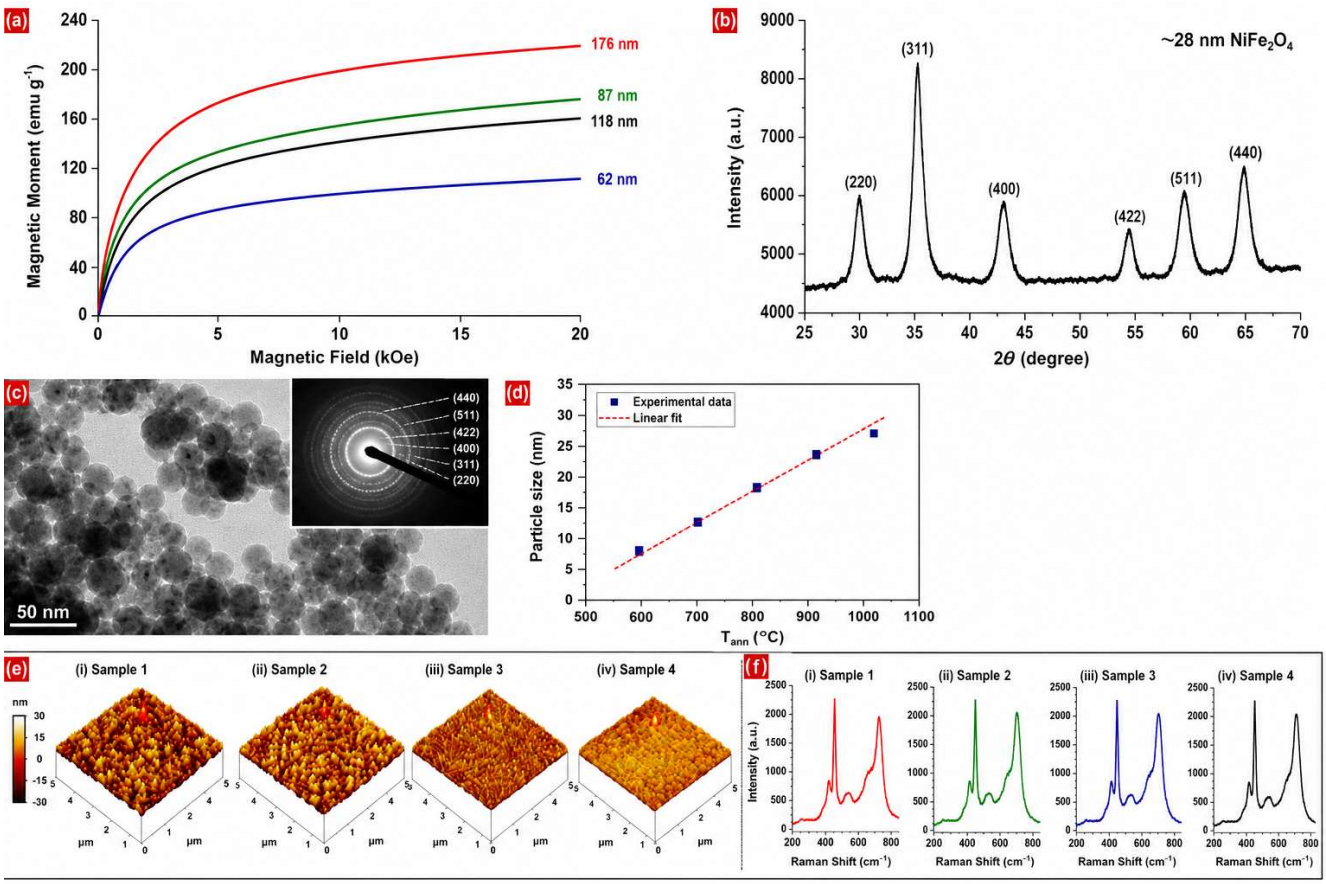


Figure 13. Pulsed laser−deposited $NiFe_2O_4$ thin films: (**a**) AFM morphology, (**b**) Raman spectra, and (**c**) room-temperature M−H curves showing the coupled evolution of topography, cation-site signatures, and magnetic response with thickness. (**d**) Linear correlation between particle size and annealing temperature, indicating thermally driven grain growth. (**e**) AFM 3D surface maps of four samples showing thickness/processing-dependent surface roughness evolution. (**f**) Raman spectra displaying the characteristic vibrational modes of spinel $NiFe_2O_4$. [5,85].

Figure 14 is a practical thickness map for sputtered $NiFe_2O_4$. The 10 nm film is structurally immature, whereas the thicker films evolve toward a continuous coarse-grained spinel layer. This microstructural transition is the practical reason why M_s increases with thickness, while H_c first rises in the finer-grained regime and then falls once grain growth and easier reversal become dominant [21,87–91].

Figure 15 confirms that the 500 nm sputtered film has already crossed into a mature continuous-film regime. The dense cross-sectional microstructure and clearer internal ordering explain why this thickness behaves differently from the 10–100 nm range. Once the film reaches this level of continuity, the dominant variables shift from nucleation deficiency to larger-scale factors such as residual strain, texture, and anti-phase-boundary density [21,87–91].

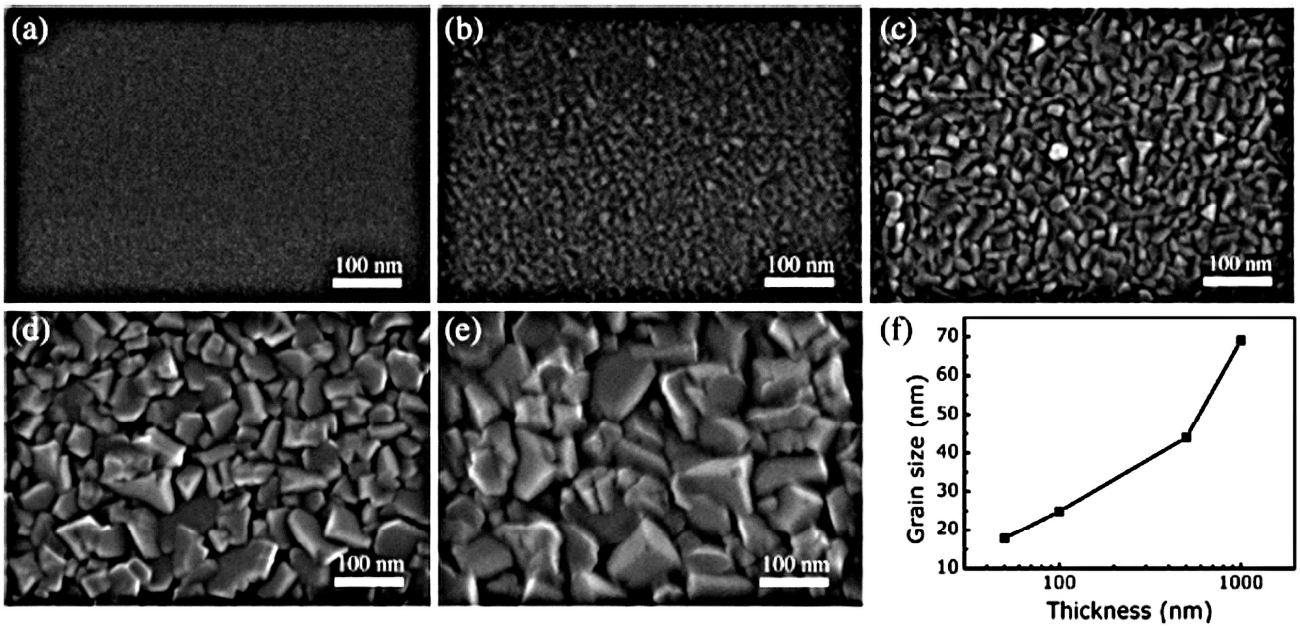


Figure 14. RF-sputtered $NiFe_2O_4$ films: SEM thickness series for 10–1000 nm films showing the morphological transition from discontinuous ultrathin coverage to continuous coarse-grained polycrystalline films: (**a**) 10 nm, (**b**) 50 nm, (**c**) 100 nm, (**d**) 500 nm, and (**e**) 1000 nm; (**f**) corresponding grain-size trend, confirming monotonic grain coarsening with increasing film thickness. [21,87–91].

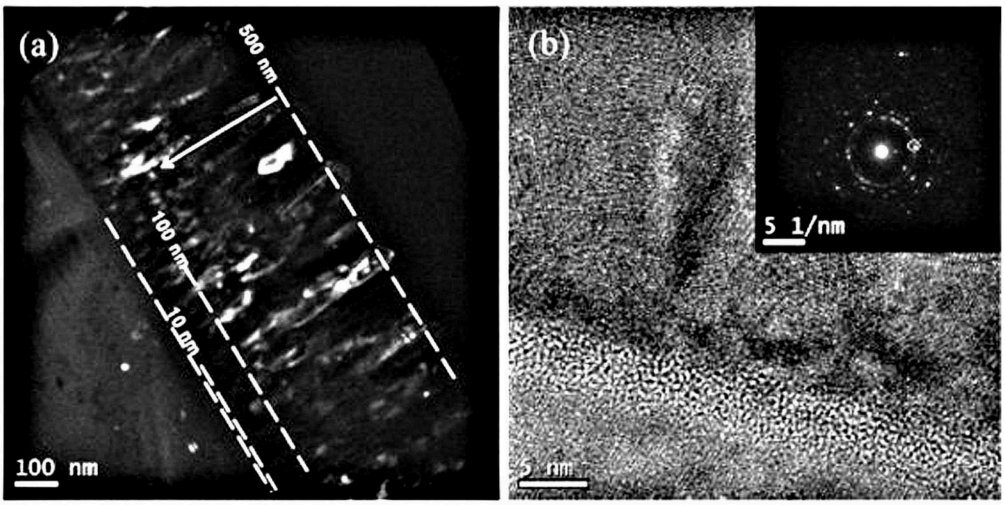


Figure 15. RF-sputtered $NiFe_2O_4$ films: TEM and HRTEM cross-sectional microstructure of the 500 nm film, showing columnar crystallization and dense film continuity at large thickness (**a**) low-magnification image showing the multilayer film region with approximate thicknesses of 500, 100, and 10 nm; (**b**) high-resolution TEM image revealing local nanocrystalline ordering, with the inset selected-area/FFT diffraction pattern confirming the polycrystalline spinel ferrite structure. [21,87–91].

Figure 16 shows that the modified-precipitation route produces a compact nanocrystalline assembly rather than the highly porous fluffy morphology common in rapid combustion products. Practically, this morphology improves measurement reproducibility and helps separate intrinsic nanoscale magnetic behavior from simple packing artifacts. It also supports the view that starch-assisted precipitation can enter the nanocrystalline regime while maintaining better morphological uniformity than many fast-chemical routes [22,92–94].

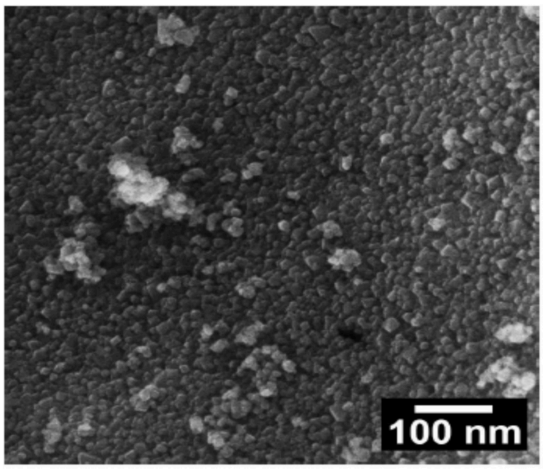


Figure 16. Modified-precipitation $NiFe_2O_4$ powder: FE-SEM microstructure of the as-prepared nanocrystalline sample, emphasizing the compact particulate morphology produced by starch-assisted precipitation [22,92–94].

Figure 17 shows what incomplete ferrite stabilization looks like in flotation-extracted $NiFe_2O_4$. The as-prepared particles remain extremely small and strongly influenced by the reaction medium, while heat treatment drives visible morphological reorganization. In practical terms, the weak magnetic response of this route is not only a size effect; it is also a crystallization problem because the starting product is far from a fully developed inverse-spinel ferrite [25,95–99].

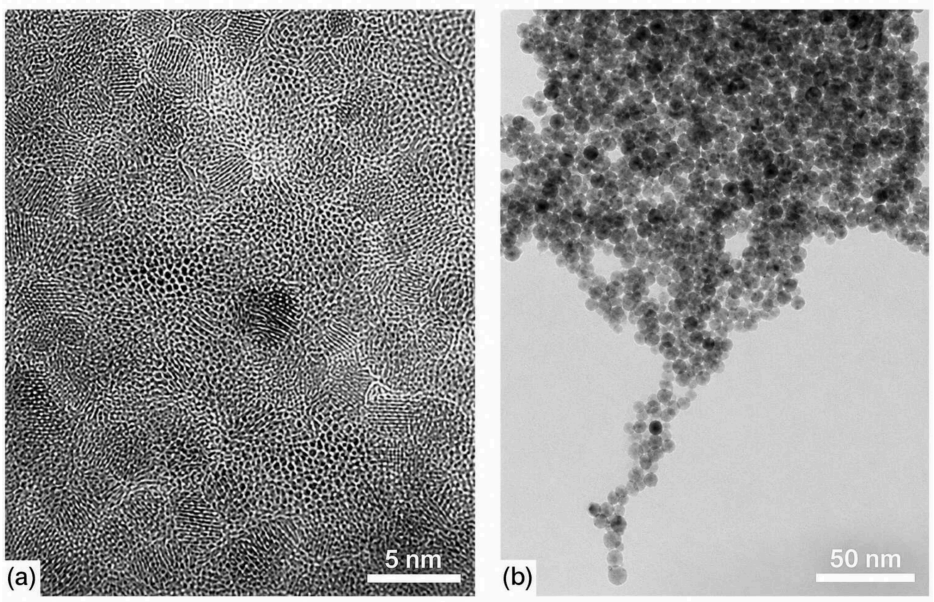


Figure 17. Flotation-extraction $NiFe_2O_4$ nanoparticles: TEM micrographs of as-prepared and heat-treated particles, showing strong morphology sensitivity to post-treatment and incomplete spinel development in the as-prepared state (**a**) high-resolution TEM image showing well-resolved lattice fringes and nanoscale crystalline domains; (**b**) low-magnification TEM image revealing agglomerated, nearly spherical nanoparticles with broad cluster formation at the tens-of-nanometers scale. [25,95–99].

Figure 18 captures the thermal trajectory of co-precipitated $NiFe_2O_4$ very clearly. Annealing sharpens the diffraction pattern, enlarges the particles, and moves the powder from a highly defective nanoparticle ensemble toward a better ordered spinel ferrite. Practically, annealing temperature is the key control knob because too little heat leaves

the phase underdeveloped, while too much heat erodes the nanoscale advantages through grain growth [26,100–103].

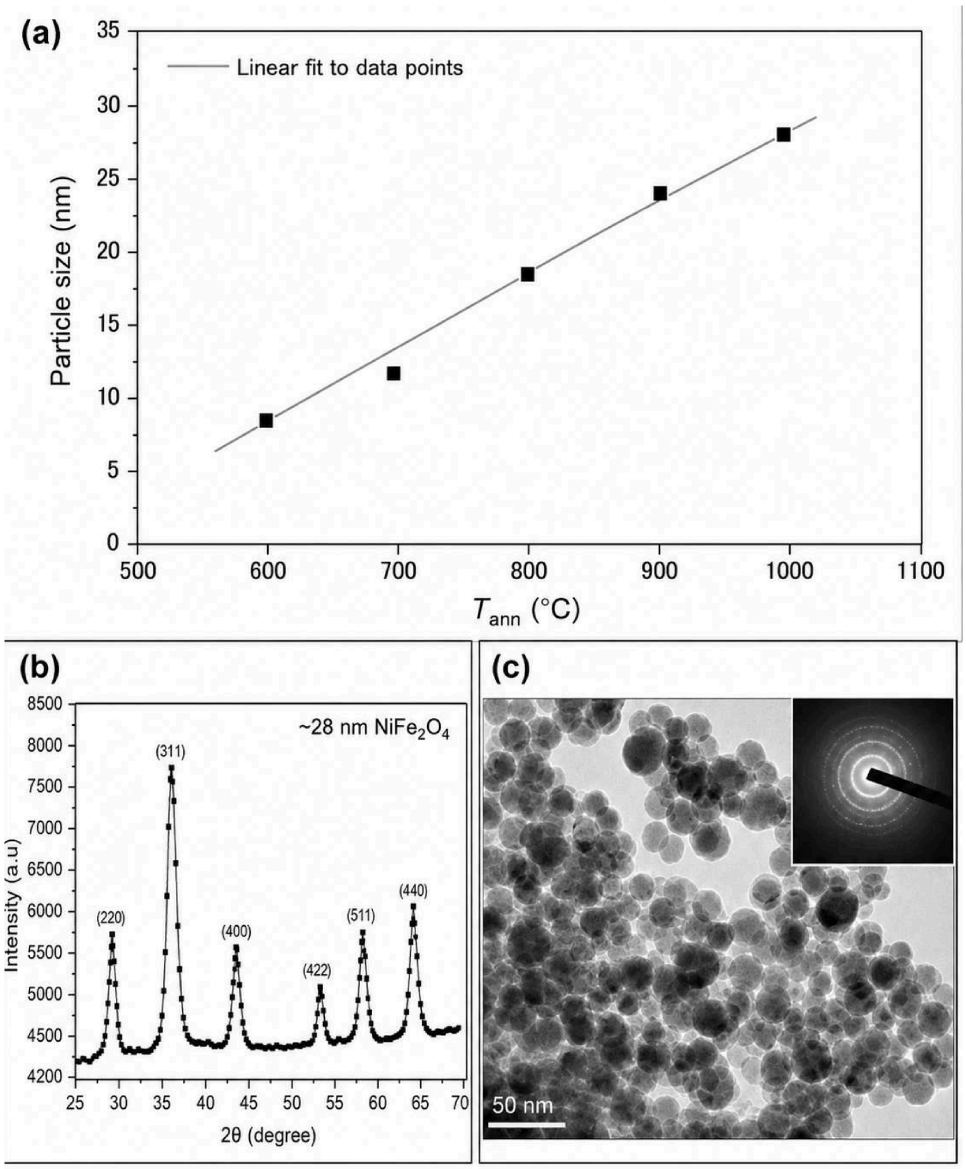


Figure 18. Co-precipitated $NiFe_2O_4$ nanoparticles: (**a**) XRD pattern, (**b**) TEM micrograph, and (**c**) particle-size versus annealing-temperature trend, showing progressive crystallization and grain growth under thermal treatment [26,100–103].

Figure 19 condenses the most important magnetic design rule in the nanoparticle regime. As particle size increases, M_s rises because the magnetically disordered surface fraction shrinks, but H_c does not rise indefinitely. Instead, coercivity passes through a maximum near the blocked single-domain window and then declines as reversal becomes easier in larger particles. For applications, this means that the best particle size depends on whether low coercivity or strong blocking is the main target [26,100–103]. Figure 15 captures the most useful magnetic design rule in the nanoparticle regime. As particle size increases, M_s rises because the magnetically disordered surface fraction decreases, but H_c does not rise indefinitely. Instead, the coercivity passes through a maximum near the single-domain window and then falls as the particles become large enough for easier magnetization reversal. The ZFC/blocking behavior reported with the same sample family supports the same interpretation. Practically, this means there is no single 'best' particle size

for all applications: soft magnetic uses favor the larger and lower-H_c side, while blocked nanoparticle uses favor the size range near the coercivity maximum [26,100–105].

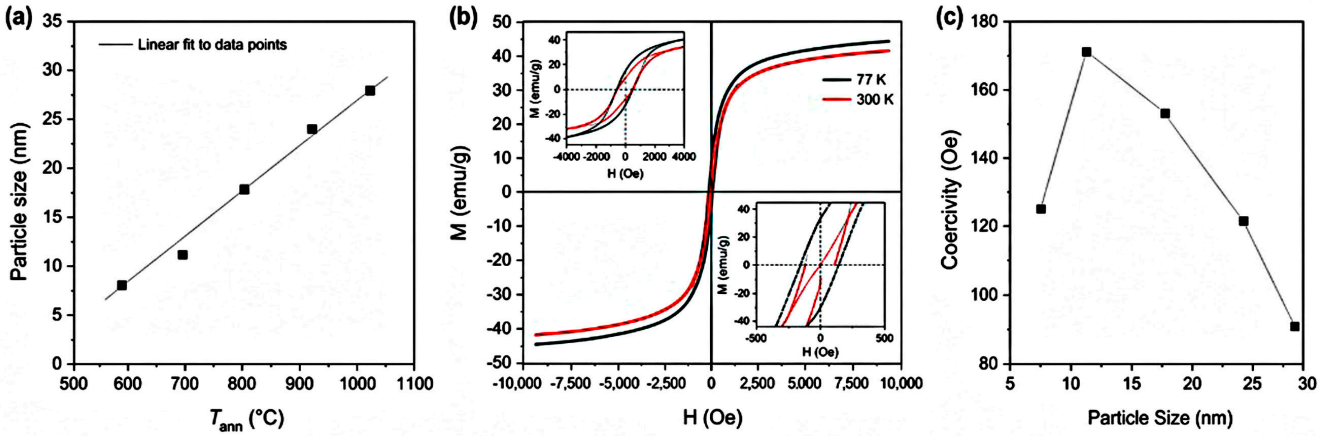


Figure 19. Size-dependent magnetic behavior of co-precipitated $NiFe_2O_4$ nanoparticles: (**a**) particle size increases nearly linearly with annealing temperature; (**b**) magnetic hysteresis loops at 77 and 300 K showing ferrimagnetic response with enhanced low-temperature magnetization and coercive opening; (**c**) coercivity varies non-monotonically with particle size, indicating competing effects of crystallinity, surface disorder, and magnetic-domain evolution l [26,100–105].

12. Applications Viewed Through Dimensionality

Nickel ferrite applications are often listed without explicit reference to dimensionality, yet dimensionality usually determines why a given form of $NiFe_2O_4$ is chosen. Bulk and thick-film ferrites are favored in classical magnetic and microwave applications because they offer stable ferrimagnetic order, high resistivity, and manageable coercivity. Nanoparticles are chosen for catalysis, separation, biomedical uses, and electrochemical applications because their surface area and field response dominate over the need for bulk-like saturation magnetization. Thin films are chosen for microelectronics and spintronics because they integrate with substrates and heterostructures [44–48,72–76,82–94,101,104–112].

A dimensionality-aware application analysis is therefore more informative than a simple list of uses. In high-frequency magnetic components, such as inductors and microwave devices, $NiFe_2O_4$ benefits from its large resistivity and moderate magnetization. Here, a bulk ceramic or a sufficiently thick and well-ordered film is generally preferable because excessive surface disorder would lower the useful permeability and increase magnetic losses. In contrast, in magnetic separation and catalysis, nanoparticle dimensionality is desirable because the accessible surface area and the ease of magnetic retrieval matter more than maximizing Ms. The same logic applies to adsorption and photocatalysis, where nanoscale $NiFe_2O_4$ is attractive even though finite-size effects suppress the moment. Biomedical applications provide another clear example. For magnetic hyperthermia, drug delivery, or MRI-related uses, one typically wants particles that can be dispersed, guided, and recovered magnetically while avoiding large remanence that would promote irreversible aggregation. Thus, weakly blocked or superparamagnetic nanoparticles are often more useful than bulk ferrites. In that application domain, the surface-disorder penalty to M_s is not purely negative; it can be part of the design space. This is one reason why the recent literature continues to emphasize co-precipitation and hydrothermal synthesis of $NiFe_2O_4$ nanoparticles for biomedical or environmental use [28,30,104]. Energy storage and catalysis also reveal a dimensionality dependence. Nanocrystalline and porous $NiFe_2O_4$ provide abundant active sites and short diffusion paths, making them useful in supercapacitors, battery anodes, and catalytic systems. Yet the same porosity and defect-rich structure that enhance these functions often reduce the magnetic coherence. Therefore, in multifunctional

systems where both electrochemical activity and magnetic recoverability matter, there is usually a trade-off between active surface area and ferrimagnetic robustness. Thin and ultrathin films are indispensable in integrated devices. Spin-filter concepts, magnetoelectric heterostructures, and oxide spintronic devices require ferrite films grown directly on single-crystal substrates or buffer layers. Here, dimensionality is tied to epitaxy, interface sharpness, and thickness-dependent anisotropy. The ultrathin-film literature is especially relevant in this context because it suggests that under carefully tuned growth conditions $NiFe_2O_4$ may exhibit unusual magnetic or electronic properties not present in the bulk. This makes ultrathin $NiFe_2O_4$ more than a curiosity; it becomes a candidate functional oxide whose properties are actively engineered by dimensionality itself. The dimensionality perspective therefore sharpens application logic. It suggests that researchers should not ask only whether $NiFe_2O_4$ is useful for a given application, but which dimensionality regime of $NiFe_2O_4$ is physically appropriate. A bulk ferrite is not simply a larger nanoparticle, and an ultrathin epitaxial film is not simply a smaller thick film. Each occupies a different point in the structure–magnetism landscape and therefore addresses a different technological need [32,33,36–40,45–55,105–110].

13. Open Questions, Limitations of the Literature, and Future Directions

Despite decades of work, the literature on $NiFe_2O_4$ still contains several unresolved questions that are best understood through the dimensionality lens developed in this review. The first concerns cation redistribution. Many papers infer inversion changes from magnetic trends alone, yet magnetization is also affected by strain, spin canting, anti-phase boundaries, and parasitic phases. Future work should therefore combine magnetometry with direct site-sensitive probes such as XAS, XMCD, Mössbauer spectroscopy, and atomically resolved microscopy whenever cation redistribution is invoked as the explanation for anomalous moments. The second unresolved problem concerns anti-phase boundaries in films. APBs are frequently mentioned but not always quantified. Yet their effect on ferrite magnetization can be so large that any serious film study should attempt either direct structural identification or indirect quantitative modeling of APB density. Without that, thickness-dependent magnetization data remain open to multiple interpretations. The same point applies to strain. It is no longer sufficient to report nominal substrate mismatch; one must distinguish coherent strain, partially relaxed strain, and defect-assisted relaxation. A third open question concerns the true intrinsic nature of the ultrathin-film enhanced-moment reports. The literature now makes clear that substrate artifacts and paramagnetic backgrounds can distort the interpretation of very thin oxide films. Future studies should therefore include systematic substrate-only controls, element-specific magnetic probes, and careful saturation analysis. The key question is not whether one specific past report was entirely right or wrong, but whether interface-stabilized inversion changes can reproducibly produce intrinsic moments above the bulk limit. This remains an important and open challenge [34,35,49,50,111].

For nanoparticles, the main unresolved issue is how to separate finite-size effects from synthesis-specific disorder. Many studies report particle size from XRD broadening alone and then relate magnetization directly to that size. However, two 10 nm $NiFe_2O_4$ samples synthesized by different methods can have very different surface chemistry, internal strain, and shell disorder. Future work should therefore integrate TEM-based size statistics, surface-sensitive spectroscopy, and temperature-dependent magnetic measurements rather than relying on average crystallite size alone [15,16,35–41,52–56,100,105].

The dimensionality framework proposed here suggests a productive strategy for future research. Instead of treating bulk, particles, fibers, films, and ultrathin films as disconnected subfields, one should deliberately design experiments that move across regimes while

holding other variables as constant as possible. For example, one could prepare $NiFe_2O_4$ by a common precursor chemistry and then convert it into bulk pellets, powders, and films, so that dimensionality changes while chemistry remains comparable. Such cross-regime studies would be particularly powerful for testing the scaling equations and regime map proposed in this review [25,26,35–43,72,73].

Another promising direction is the coupling of dimensionality with external stimuli. Strain, electric field, light, and chemical environment may all alter cation distribution or spin order in reduced-dimensional $NiFe_2O_4$. If interface-sensitive ultrathin films can be stabilized reproducibly, the possibility of tuning their magnetism dynamically becomes especially interesting [26,29]. Likewise, the combination of nanoparticle surface engineering with controlled blocking temperatures could produce optimized materials for biomedical or environmental applications [27,28,30,112].

A final limitation in the literature is linguistic rather than experimental: many papers still discuss nickel ferrite using generic ferrite language without distinguishing which phenomena are actually specific to $NiFe_2O_4$. The present review argues that $NiFe_2O_4$ deserves more tailored interpretation because its moderate anisotropy, inverse-spinel chemistry, and sensitivity to nonequilibrium inversion place it in a particularly rich dimensionality landscape. Recognizing this specificity is necessary if the field is to move from empirical observation toward predictive design [1–8,20,25,26,72,73].

14. Conclusions

This review has re-examined nickel ferrite from the viewpoint of dimensionality and has argued that dimensionality is the master variable governing the relationship between structure and magnetic properties in $NiFe_2O_4$. The main conclusion is that $NiFe_2O_4$ does not possess a single magnetic identity independent of size, thickness, morphology, or synthesis route. Instead, the measured magnetic behavior emerges from a competition among equilibrium inverse-spinel ferrimagnetism, cation redistribution, microstructural coherence, and surface/interface spin disorder.

Bulk $NiFe_2O_4$ serves as the equilibrium reference state: a near-inverse-spinel ferrimagnet with moderate saturation magnetization, high resistivity, and high Curie temperature. Nanoparticles depart from this state because their disordered surface shell occupies an increasingly large fraction of the volume, which suppresses M_s and T_C and drives the system toward blocking or superparamagnetic behavior. One-dimensional nanostructures add shape anisotropy and show that morphology itself is a dimensionality variable. Thin films form a separate regime controlled by thickness, strain, texture, and anti-phase boundaries; their magnetic properties cannot be understood from size arguments alone. Ultrathin epitaxial films constitute the most extreme and controversial limit, in which interface-driven nonequilibrium inversion and reconstruction may even produce moments beyond the bulk expectation under specific growth conditions [1–8,15–18,25,26,28–30].

A major novelty of this article is the proposal of a three-function theoretical framework for interpreting the literature: the cation-distribution function, the microstructural coherence function, and the surface/interface spin-order parameter. This framework explains why the magnetic response of $NiFe_2O_4$ changes in different ways across bulk ceramics, nanocrystalline powders, one-dimensional nanostructures, ordinary thin films, and ultrathin epitaxial layers. It also clarifies why synthesis route must be treated as part of the dimensionality problem rather than as a separate methodological detail [10–18,25,26,28–34,42].

From an application perspective, the key conclusion of this review is that $NiFe_2O_4$ should be selected and engineered according to dimensionality rather than composition alone. Bulk ceramics are best suited for stable magnetic and high-frequency uses, nanopar-

ticles for surface-driven environmental, biomedical, catalytic, and electrochemical applications, one-dimensional structures for anisotropic and aligned architectures, and thin or ultrathin films for integrated spintronic and magnetoelectric devices. Future progress will therefore depend on matching the dimensionality-controlled magnetic state to the target function while controlling cation inversion, crystallinity, surface disorder, strain, and interface quality. The corresponding dimensionality-dependent application directions and principal design limitations are summarized in Appendix A, Table A2.

The literature surveyed here, including the two uploaded attachments and the broader internet-based journal record, strongly supports one overarching conclusion: dimensionality in nickel ferrite is not a secondary correction to a bulk ferrite model. It is the central organizing principle of the field. Any future attempt to optimize $NiFe_2O_4$ for magnetic, electronic, catalytic, or biomedical applications must therefore begin by choosing the appropriate dimensionality regime and understanding the structural perturbations that regime introduces. That is the most robust lesson to emerge from the present review and the clearest path forward for future nickel ferrite research [72–76,82–94,101,103,104,106–112].

Author Contributions: Conceptualization, M.A. and T.A.; methodology, M.A. and T.A.; software, M.A. and T.A.; validation, M.A. and T.A.; formal analysis, M.A., T.A., Y.M. and J.M.; investigation, M.A. and T.A.; resources, M.A. and T.A.; data curation, M.A. and T.A.; writing—original draft, M.A. and T.A.; writing—review and editing, M.A. and T.A.; visualization, M.A. and T.A.; supervision, M.A. and T.A.; project administration, M.A. and T.A. All authors have read and agreed to the published version of the manuscript.

Funding: This research received no external funding.

Institutional Review Board Statement: Not applicable.

Informed Consent Statement: Not applicable.

Data Availability Statement: The original contributions presented in this study are included in the article. Further inquiries can be directed to the corresponding author(s).

Conflicts of Interest: The authors declare no conflict of interest.

Appendix A

Table A1. Comparative perspective on major synthesis routes.

Method	Main Dimensionality Regime Accessed	Key Strengths	Typical Magnetic/Structural Penalty
Solid-state ceramic reaction	Bulk/coarse polycrystals	Near-equilibrium spinel; robust reference values	Large grains, limited nanoscale control
Ball milling/reactive milling	Nanocrystalline powders	Simple, scalable, strong finite-size access	High strain, contamination risk, broad disorder
Co-precipitation/precipitation	Nanoparticles	Low temperature, scalable chemistry	Agglomeration and post-anneal sensitivity
Hydrothermal/solvothermal	Nanoparticles and 1D forms	Good crystallinity and shape control	Autoclave complexity; pressure dependence
Combustion	Highly porous nanopowders	Fast and energy-efficient	Broad size distribution and local inhomogeneity
PLD	Thin films and ultrathin epitaxial films	Excellent thickness control, stoichiometric transfer	Costly; highly parameter sensitive
RF sputtering	Thin films	Industrial relevance and uniform deposition	Often requires annealing; APBs/strain remain critical

Table A2. Dimensionality-dependent application directions and key design limitations of $NiFe_2O_4$ materials.

$NiFe_2O_4$ Form/Dimensionality Regime	Key Dimensionality-Controlled Feature	Most Suitable Application Directions	Main Limitation to Control
Bulk/near-bulk ceramics	Stable inverse-spinel ferrimagnetism; high resistivity; moderate coercivity; thermal robustness	High-frequency ferrite components; microwave devices; inductive elements; reference magnetic materials	Large grain size and limited surface functionality
Nanoparticles/nanocrystalline powders	High surface-to-volume ratio; surface spin canting; possible superparamagnetism; high interfacial activity	Magnetic separation; hyperthermia; catalysis; adsorption; environmental remediation; battery and supercapacitor electrodes	Suppressed M_s, aggregation, broad size distribution, and spin disorder
One-dimensional nanostructures	Shape anisotropy; directional magnetic/electronic pathways; enhanced alignment under external fields	Anisotropic sensors; microwave absorbers; field-guided assemblies; aligned electrode networks	Radial surface disorder and weak intergrain coupling
Polycrystalline thin films	Thickness-dependent strain, texture, grain boundaries, and anti-phase-boundary effects	Integrated magnetic sensors; microwave thin-film components; magnetoelectric heterostructures	Defect-rich interfaces and incomplete saturation
Ultrathin epitaxial films	Interface-driven strain, cation redistribution, and electronic reconstruction	Spin filters; oxide spintronics; interface-engineered magnetic devices	Substrate contribution, anti-phase boundaries, and difficulty separating intrinsic/extrinsic effects

References

1. Smit, J.; Wijn, H.P.J. *Ferrites: Physical Properties of Ferrimagnetic Oxides in Relation to Their Technical Applications*; John Wiley & Sons: New York, NY, USA, 1959.
2. Cullity, B.D.; Graham, C.D. *Introduction to Magnetic Materials*, 2nd ed.; Wiley-IEEE Press: Hoboken, NJ, USA, 2008.
3. O'Handley, R.C. *Modern Magnetic Materials: Principles and Applications*; John Wiley & Sons: New York, NY, USA, 2000.
4. Goldman, A. *Modern Ferrite Technology*, 2nd ed.; Springer: New York, NY, USA, 2006.
5. Valenzuela, R. *Magnetic Ceramics*; Cambridge University Press: Cambridge, UK, 1994.
6. Coey, J.M.D. *Magnetism and Magnetic Materials*; Cambridge University Press: Cambridge, UK, 2010.
7. Chikazumi, S. *Physics of Ferromagnetism*, 2nd ed.; Graham, C.D., Jr., Ed.; Oxford University Press: Oxford, UK, 1997.
8. Kittel, C. *Introduction to Solid State Physics*, 8th ed.; John Wiley & Sons: Hoboken, NJ, USA, 2005.
9. Klewe, C.; Meinert, M.; Boehnke, A.; Kuepper, K.; Arenholz, E.; Gupta, A.; Schmalhorst, J.-M.; Kuschel, T.; Reiss, G. Physical characteristics and cation distribution of $NiFe_2O_4$ thin films with high resistivity prepared by reactive co-sputtering. *J. Appl. Phys.* **2014**, *115*, 123903. [CrossRef]
10. Anderson, P.W. Antiferromagnetism. Theory of superexchange interaction. *Phys. Rev.* **1950**, *79*, 350–356. [CrossRef]
11. Goodenough, J.B. Theory of the role of covalence in the perovskite-type manganites [La, M(II)]MnO_3. *Phys. Rev.* **1955**, *100*, 564–573. [CrossRef]
12. Yafet, Y.; Kittel, C. Antiferromagnetic arrangements in ferrites. *Phys. Rev.* **1952**, *87*, 290–294. [CrossRef]
13. Smart, J.S. The Néel theory of ferrimagnetism. *Am. J. Phys.* **1955**, *23*, 356–370. [CrossRef]
14. Gorter, E.W. Saturation magnetization and crystal chemistry of ferrimagnetic oxides. *Philips Res. Rep.* **1954**, *9*, 295–320.
15. Dormann, J.L.; Fiorani, D.; Tronc, E. Magnetic relaxation in fine-particle systems. In *Advances in Chemical Physics*; John Wiley & Sons: New York, NY, USA, 1997; Volume 98, pp. 283–494.
16. Kodama, R.H. Magnetic nanoparticles. *J. Magn. Magn. Mater.* **1999**, *200*, 359–372. [CrossRef]
17. Stoner, E.C.; Wohlfarth, E.P. A mechanism of magnetic hysteresis in heterogeneous alloys. *Philos. Trans. R. Soc. London. Ser. A Math. Phys. Sci.* **1948**, *240*, 599–642. [CrossRef]
18. Bean, C.P.; Livingston, J.D. Superparamagnetism. *J. Appl. Phys.* **1959**, *30*, S120–S129. [CrossRef]
19. Morrish, A.H. *The Physical Principles of Magnetism*; Wiley-IEEE Press: Piscataway, NJ, USA, 2001.
20. Sickafus, K.E.; Wills, J.M.; Grimes, N.W. Structure of spinel. *J. Am. Ceram. Soc.* **1999**, *82*, 3279–3292. [CrossRef]
21. Gilleo, M.A. Superexchange interaction in ferrimagnetic garnets and spinels which contain randomly incomplete linkages. *J. Phys. Chem. Solids* **1960**, *13*, 33–39. [CrossRef]
22. Blasse, G. Crystal chemistry and some magnetic properties of mixed metal oxides with spinel structure. *Philips Res. Rep. Suppl.* **1964**, *3*, 1–139.
23. Sugimoto, M. The past, present, and future of ferrites. *J. Am. Ceram. Soc.* **1999**, *82*, 269–280. [CrossRef]
24. Berkowitz, A.E.; Schuele, W.J. Magnetic properties of some ferrite micropowders. *J. Appl. Phys.* **1959**, *30*, S134–S135. [CrossRef]

25. Néel, L. Propriétés magnétiques des ferrites; ferrimagnétisme et antiferromagnétisme. *Ann. Phys.* **1948**, *12*, 137–198. [CrossRef]
26. Prasad, B.V. Effect of indium substitution on the electrical and magnetic properties of Ni-Zn ferrites. *J. Theor. Appl. Phys.* **2015**, *9*, 267–272. [CrossRef]
27. Zeng, X.; Zhang, J.; Zhu, S.; Deng, X.; Ma, H.; Zhang, J.; Zhang, Q.; Li, P.; Xue, D.; Mellors, N.J.; et al. Direct observation of cation distributions of ideal inverse spinel $CoFe_2O_4$ nanofibres and correlated magnetic properties. *Nanoscale* **2017**, *9*, 7493–7500. [CrossRef] [PubMed]
28. Lüders, U.; Bibes, M.; Bobo, J.-F.; Cantoni, M.; Bertacco, R.; Fontcuberta, J. Enhanced magnetic moment and conductive behavior in $NiFe_2O_4$ spinel ultrathin films. *Phys. Rev. B* **2005**, *571*, 134419.
29. Foerster, M.; Rebled, J.M.; Estradé, S.; Sánchez, F.; Peiró, F.; Fontcuberta, J. Distinct magnetism in ultrathin epitaxial $NiFe_2O_4$ films on $MgAl_2O_4$ and $SrTiO_3$ single crystalline substrates. *Phys. Rev. B—Condens. Matter Mater. Phys.* **2011**, *84*, 144422.
30. Saha, S.; Knut, R.; Gupta, A.; Radu, F.; Luo, C.; Karis, O.; Arena, D.A. Near-surface electronic structure in strained Ni-ferrite films: An x-ray absorption spectroscopy study. *J. Vac. Sci. Technol. A* **2024**, *42*, 012702. [CrossRef]
31. Caltun, O.F. Pulsed laser deposition of $NiFe_2O_4$ thin films. *J. Optoelectron. Adv. Mater.* **2004**, *6*, 935–938.
32. Dixit, G.; Singh, J.; Srivastava, R.; Agrawal, H.; Chaudhary, R. Structural, magnetic and optical studies of nickel ferrite thin films. *Adv. Mater. Lett.* **2012**, *3*, 21–28. [CrossRef]
33. Dong, C.; Wang, G.; Guo, D.; Jiang, C.; Xue, D. Growth, structure, morphology, and magnetic properties of Ni ferrite films. *Nanoscale Res. Lett.* **2013**, *8*, 196. [CrossRef] [PubMed]
34. Datta, R.; Loukya, B.; Li, N.; Gupta, A. Structural features of epitaxial $NiFe_2O_4$ thin films grown on different substrates by direct liquid injection chemical vapor deposition. *J. Cryst. Growth* **2012**, *345*, 44–50. [CrossRef]
35. Maaz, K.; Karim, S.; Mumtaz, A.; Hasanain, S.K.; Liu, J.; Duan, J.L. Synthesis and magnetic characterization of nickel ferrite nanoparticles prepared by co-precipitation route. *J. Magn. Magn. Mater.* **2009**, *321*, 1838–1842. [CrossRef]
36. Nejati, K.; Zabihi, R. Preparation and magnetic properties of nano size nickel ferrite particles using hydrothermal method. *Chem. Cent. J.* **2012**, *6*, 23. [CrossRef] [PubMed]
37. Nabiyouni, G.; Fesharaki, M.J.; Mozafari, M.; Amighian, J. Characterization and magnetic properties of nickel ferrite nanoparticles prepared by ball milling technique. *Chin. Phys. Lett.* **2010**, *27*, 126401. [CrossRef]
38. Marinca, T.; Chicinaş, I.; Isnard, O.; Pop, V.; Popa, F. Synthesis, structural and magnetic characterization of nanocrystalline nickel ferrite—$NiFe_2O_4$ obtained by reactive milling. *J. Alloys Compd.* **2011**, *509*, 7931–7936. [CrossRef]
39. Chireh, M.; Naseri, M.; Kamalianfar, A. ^{57}Fe Mössbauer spectroscopy investigation of $NiFe_2O_4$ and $MnFe_2O_4$ ferrite nanoparticles prepared by thermal treatment method. *Appl. Phys. A* **2020**, *126*, 543. [CrossRef]
40. Oshtrakh, M.I.; Ushakov, M.V.; Senthilkumar, B.; Selvan, R.K.; Sanjeeviraja, C.; Felner, I.; Semionkin, V.A. Study of $NiFe_2O_4$ nanoparticles using Mössbauer spectroscopy with a high velocity resolution. *Hyperfine Interact.* **2013**, *219*, 7–12. [CrossRef]
41. Poddar, A.; Bhowmik, R.N.; De, A.; Sen, P. Magnetic response of $NiFe_2O_4$ nanoparticles in polymer matrix. *J. Magn. Magn. Mater.* **2009**, *321*, 2015–2020.
42. Regmi, S.; Singh, A.V.; Khodadadi, B.; Mohammadi, J.B.; Keshavarz, S.; Mewes, T.; Gupta, A. Structural and magnetic properties of $NiFe_2O_4$ thin films grown on isostructural lattice-matched substrates. *Appl. Phys. Lett.* **2021**, *118*, 152402. [CrossRef]
43. Nguyet, D.T.T.; Duong, N.P.; Hung, L.T.; Hien, T.D.; Satoh, T. Crystallization and magnetic behavior of nanosized nickel ferrite prepared by citrate precursor method. *J. Alloys Compd.* **2011**, *509*, 6621–6625. [CrossRef]
44. Raj, K.; Moskowitz, B.; Casciari, R. Advances in ferrofluid technology. *J. Magn. Magn. Mater.* **1995**, *149*, 174–180. [CrossRef]
45. Pankhurst, Q.A.; Connolly, J.; Jones, S.K.; Dobson, J. Applications of magnetic nanoparticles in biomedicine. *J. Phys. D Appl. Phys.* **2003**, *36*, R167–R181. [CrossRef]
46. Hergt, R.; Dutz, S.; Müller, R.; Zeisberger, M. Magnetic particle hyperthermia: Nanoparticle magnetism and ma-terials development for cancer therapy. *J. Phys. Condens. Matter* **2006**, *18*, S2919–S2934.
47. Tartaj, P.; Morales, M.P.; Veintemillas-Verdaguer, S.; González-Carreño, T.; Serna, C.J. The preparation of magnetic nanoparticles for applications in biomedicine. *J. Phys. D Appl. Phys.* **2003**, *36*, R182–R197. [CrossRef]
48. Sun, S.; Zeng, H.; Robinson, D.B.; Raoux, S.; Rice, P.M.; Wang, S.X.; Li, G. Monodisperse mFe_2O_4 (m = Fe, Co, Mn) nanoparticles. *J. Am. Chem. Soc.* **2004**, *126*, 273–279. [PubMed]
49. Rao, C.N.R.; Müller, A.; Cheetham, A.K. (Eds.) *The Chemistry of Nanomaterials: Synthesis, Properties and Applications*; Wiley-VCH: Weinheim, Germany, 2004; Volume 2.
50. Burda, C.; Chen, X.; Narayanan, R.; El-Sayed, M.A. Chemistry and properties of nanocrystals of different shapes. *Chem. Rev.* **2005**, *105*, 1025–1102. [CrossRef] [PubMed]
51. Laurent, S.; Forge, D.; Port, M.; Roch, A.; Robic, C.; Vander Elst, L.; Muller, R.N. Magnetic iron oxide nanoparticles: Synthesis, stabilization, vectorization, physicochemical characterizations, and biological applications. *Chem. Rev.* **2008**, *108*, 2064–2110. [CrossRef] [PubMed]
52. Gleiter, H. Nanocrystalline materials. *Prog. Mater. Sci.* **1989**, *33*, 223–315. [CrossRef]
53. Suryanarayana, C. Mechanical alloying and milling. *Prog. Mater. Sci.* **2001**, *46*, 1–184. [CrossRef]

54. Suryanarayana, C.; Al-Aqeeli, N. Mechanically alloyed nanocomposites. *Prog. Mater. Sci.* **2013**, *58*, 383–502. [CrossRef]
55. A Majetich, S.; Sachan, M. Magntostatic interactions in magnetic nanoparticle assemblies: Energy, time and length scales. *J. Phys. D. Appl. Phys.* **2006**, *39*, R407–R422.
56. Leslie-Pelecky, D.L.; Rieke, R.D. Magnetic properties of nanostructured materials. *Chem. Mater.* **1996**, *8*, 1770–1783. [CrossRef]
57. Berkowitz, A.E.; Kodama, R.H.; Makhlouf, S.A.; Parker, F.T.; Spada, F.E.; McNiff, E.J., Jr.; Foner, S. Anomalous properties of magnetic nanoparticles. *J. Magn. Magn. Mater.* **1999**, *196*, 591–594. [CrossRef]
58. Néel, L. Some theoretical aspects of rock-magnetism. *Adv. Phys.* **1955**, *4*, 191–243. [CrossRef]
59. Chantrell, R.W.; Popplewell, J.; Charles, S.W. Measurements of particle size distribution parameters in ferrofluids. *IEEE Trans. Magn.* **1978**, *14*, 975–977. [CrossRef]
60. Massart, R. Preparation of aqueous magnetic liquids in alkaline and acidic media. *IEEE Trans. Magn.* **1981**, *17*, 1247–1248. [CrossRef]
61. Peddis, D.; Yaacoub, N.; Ferretti, M.; Martinelli, A.; Piccaluga, G.; Musinu, A.; Cannas, C.; Navarra, G.; Greneche, J.M.; Fiorani, D. Cationic distribution and spin canting in $CoFe_2O_4$ nanoparticles. *J. Phys. Condens. Matter* **2011**, *23*, 426004. [CrossRef] [PubMed]
62. Maensiri, S.; Masingboon, C.; Boonchom, B.; Seraphin, S. A simple route to synthesize nickel ferrite ($NiFe_2O_4$) nanoparticles using egg white. *Scr. Mater.* **2007**, *56*, 797–800. [CrossRef]
63. Saensuk, O.; Phokha, S.; Bootchanont, A.; Maensiri, S.; Swatsitang, E. Fabrication and magnetic properties of $NiFe_2O_4$ nanofibers obtained by electrospinning. *Ceram. Int.* **2015**, *41*, 8133–8141. [CrossRef]
64. Sun, L.; Zhang, R.; Wang, Z.; Ju, L.; Cao, E.; Zhang, Y. Structural, dielectric and magnetic properties of NiFe2O4 prepared via sol–gel auto-combustion method. *J. Magn. Magn. Mater.* **2017**, *421*, 65–70. [CrossRef]
65. Zhang, Y.; Qu, H.; Gang, C.; Guan, H.; Dong, C.; Yin, Z. Porous, Tremella-like NiFe2O4 with ultrathin nanosheets for ppb-Level toluene detection. *Crystals* **2023**, *13*, 865.
66. Komarneni, S.; D'Arrigo, M.C.; Leonelli, C.; Pellacani, G.C.; Katsuki, H. Microwave-hydrothermal synthesis of nanophase ferrites. *J. Am. Ceram. Soc.* **1998**, *81*, 3041–3043. [CrossRef]
67. Gabal, M.A.; Al Angari, Y.M. Effect of diamagnetic substitution on the structural, magnetic and electrical properties of NiFe2O4. *Mater. Chem. Phys.* **2009**, *115*, 578–584. [CrossRef]
68. Morrison, S.A.; Cahill, C.L.; Carpenter, E.E.; Calvin, S.; Swaminathan, R.; McHenry, M.E.; Harris, V.G. Magnetic and structural properties of nickel zinc ferrite nanoparticles synthesized at room temperature. *J. Appl. Phys.* **2004**, *95*, 6392–6395. [CrossRef]
69. Majid, F.; Rauf, J.; Ata, S.; Bibi, I.; Malik, A.; Ibrahim, S.M.; Ali, A.; Iqbal, M. Synthesis and characterization of $NiFe_2O_4$ ferrite: Sol-gel and hydrothermal synthesis routes effect on magnetic, structural and dielectric characteristics. *Mater. Chem. Phys.* **2021**, *258*, 123888. [CrossRef]
70. Yildirim, S.; Ozler, B.; Ozdemir, E.T.; Erol, M.; Dikici, T.; Oguzlar, S. The structural, magnetic, and optical properties of flame spray pyrolysis-derived spinel $NiFe_2O_4$ nanoparticles. *J. Am. Ceram. Soc.* **2025**, *108*, e20220.
71. Wen, J.; Yang, J.; Liu, C.; He, Z.; Gao, L. Synthesis and magnetic properties of spinel $NiFe_2O_4$ nanoparticles by oxidation roasting technique. *Mater. Sci. Eng. B* **2025**, *319*, 118375. [CrossRef]
72. Patra, J.; Verma, V.K. Nickel ferrite: Advances in the synthesis methods, properties and its applications. *Nano-Struct. Nano-Objects* **2025**, *42*, 101458. [CrossRef]
73. Chetia, T.; Suleman, A.; Chetia, B. A comprehensive review on magnetic $NiFe_2O_4$ nanoparticles: Synthesis approaches and catalytic proficiency in various coupling reactions. *Tetrahedron* **2024**, *164*, 134172. [CrossRef]
74. Mushtaq, M.W.; Shahbaz, M.; Naeem, R.; Bashir, S.; Sharif, S.; Ali, K.; Dogar, N.A. Synthesis of surfactant-assisted nickel ferrite nanoparticles (NFNPs@ surfactant) to amplify their application as an advanced electrode material for high-performance supercapacitors. *RSC Adv.* **2024**, *14*, 20230–20239. [CrossRef] [PubMed]
75. Krishnan, A.A.; Harikumar, S.; Kumar, M.A.A.; Nair, R.B.; Kurian, S.; Sha, M.A.; Arun, P.S. $NiFe_2O_4$: Harnessing catalytic potential in water splitting. *Catal. Sci. Technol.* **2024**, *14*, 6155–6175. [CrossRef]
76. Askari, M.B.; Salarizadeh, P.; Moghadam, M.T.T. $NiFe_2O_4$ as a promising electrode material: A comprehensive review on supercapacitor applications. *Fuel* **2026**, *403*, 136104. [CrossRef]
77. Patra, J.; Parida, P.; Patel, P.; Sahoo, S.K.; Parvin, K.; Babu, B.J.; Amemiya, K.; Kandasami, A.; Singh, V.R.; Verma, V.K. Tailoring electronic structure and magnetic anisotropy in spray-pyrolyzed $NiFe_2O_4$ thin films for spintronic applications. *Sci. Rep.* **2026**, *16*, 13485. [CrossRef] [PubMed]
78. Boussafel, H.; Sedrati, C.; Alleg, S. Green synthesis of $NiFe_2O_4$, $CoFe_2O_4$, and $Ni_{0.5}Co_{0.5}Fe_2O_4$ by sol-gel autocombustion method using olive leaf extract as fuel. *Appl. Phys. A* **2024**, *130*, 374. [CrossRef]
79. Roostaei, S.; Ahmadi-Kashani, M.; Salavati-Niasari, M.; Alsultany, F.H. Designing a novel highly efficient magnetic binary $NiFe_2O_4/CeO_2$ nano-photocatalyst for visible-light-driven degradation of organic pollutants. *Appl. Water Sci.* **2025**, *15*, 127. [CrossRef]
80. Koca, F.D.; Sahin, B. Green synthesis of $NiFe_2O_4$ nanoparticles and evaluation of their photocatalytic activities. *Inorg. Nano-Met. Chem.* **2025**, *55*, 977–983. [CrossRef]

81. Barzegar, A.; Ebrahimzadeh, S.; Haeili, M.; Shoghi, Y.; Ahmadi, A. Green-synthesized magnetic core-shell $NiFe_2O_4$@Ag nanoparticles enhance antibiotic efficacy against nosocomial pathogens. *Biochem. Biophys. Rep.* **2025**, *43*, 102121. [CrossRef] [PubMed]
82. Kharat, P.B.; Somvanshi, S.B.; Dawi, E.A.; Ibrahim, R.M.; Mopari, A.M. Surface-functionalized nanoscale nickel-ferrites ($NiFe_2O_4$) nanoparticles as heating agents for cancer theranostics. *Inorg. Chem. Commun.* **2025**, *182*, 115569. [CrossRef]
83. Stambouli, G.B.; Benguella, B.; Benamar, M.; Kamel, A.H. Polymer-enhanced nickel ferrite catalyst for the efficient reduction of 4-nitrophenol as a hazard pollutant. *Environ. Sci. Adv.* **2025**, *4*, 1684–1698. [CrossRef]
84. Raj, R.; Paswan, S.K.; Kumar, L.; Singh, G.P.; Haldar, K.K. $Ti_3C_2T_x$ nanosheet/$NiFe_2O_4$ nanoparticle composites for electrocatalytic water splitting. *ACS Appl. Nano Mater.* **2025**, *8*, 1649–1661. [CrossRef]
85. Sumithanandhi, S.; Pari, S.; Muthupandi, S.; Kasinathan, K.; Joselene Suzan Jennifer, P. Enhanced electrochemical characteristics of rGO incorporated $NiFe_2O_4$ nanorods electrode structure for supercapacitor applications. *Results Surf. Interfaces* **2026**, *23*, 100756. [CrossRef]
86. Vahedrouz, F.; Alizadeh, M.; Bahrami, A.; Laybidi, F.H. Magnetic behavior of Co^{2+}-doped $NiFe_2O_4$ nanoparticles with single-phase spinel structure. *Crystals* **2025**, *15*, 624. [CrossRef]
87. Baytar, O.; Ekinci, A.; Sahin, O.; Akdag, A. The use of $NiFe_2O_4$ and $CoFe_2O_4$ nanoparticles produced by green synthesis as electrode material for supercapacitors. *ChemistrySelect* **2024**, *9*, e202304491. [CrossRef]
88. Al-Shuayfani, S.A.; Gunday, S.T.; Cevik, E.; Almessiere, M.A.; Caliskan, S.; Baykal, A. Dual-window electrochemical application of a MoS_2@$NiFe_2O_4$ spinel hybrid heterostructure: High-performance asymmetric and symmetric supercapacitors. *Chem.—Asian J.* **2026**, *21*, e70575. [CrossRef] [PubMed]
89. Fadhel, S.R.; Dhaif, S.R.; Jasim, Z.A.; Mohammad, A.S.; Balakit, A.A.; Al-Jubouri, R.K.M. Chitosan–$NiFe_2O_4$ nanocomposite synthesis for effective removal of Pb(II) and Zn(II) ions from water. *Results Chem.* **2024**, *11*, 101776.
90. Chaudhari, N.U.; Jagadale, S.K.; Patil, R.S.; Dusane, P.R.; More, Y.S.; Kute, M.B.; Bankar, P.K.; Rathod, S.M. Nanostructured Mo-doped $NiFe_2O_4$: A promising electrode materials for supercapacitor with improved charge storage capacity. *Solid State Sci.* **2025**, *168*, 108033. [CrossRef]
91. El-Masry, M.M.; Arman, M.M. Cobalt, nickel and zinc spinel ferrites with high transmittance and UV-blocking for advanced optical applications. *Sci. Rep.* **2025**, *15*, 16636. [CrossRef] [PubMed]
92. Ghaffar, D.N.; Arman, M.; El-Dek, S.I.; Ramadan, R. Studying the preparation; characterization, and physical properties of $NiFe_2O_4$, TiO_2, and $NiFe_2O_4$/TiO_2 nanocomposite. *Appl. Phys. A* **2024**, *130*, 164. [CrossRef]
93. Kefeni, K.K.; Mamba, B.B.; Msagati, T.A.M. Application of spinel ferrite nanoparticles in water and wastewater treatment: A review. *Sep. Purif. Technol.* **2017**, *188*, 399–422. [CrossRef]
94. Yadav, R.S.; Kuřitka, I. Spinel ferrite and MXene-based magnetic novel nanocomposites: An innovative high-performance electromagnetic interference shielding and microwave absorber. *Crit. Rev. Solid State Mater. Sci.* **2023**, *48*, 441–479.
95. Humbe, A.V.; Kounsalye, J.S.; Somvanshi, S.B.; Kumar, A.; Jadhav, K.M. Cation distribution, magnetic and hyperfine interaction studies of Ni–Zn spinel ferrites: Role of Jahn–Teller ion (Cu^{2+}) substitution. *Mater. Adv.* **2020**, *1*, 880–890. [CrossRef]
96. Thakur, S.; Katyal, S.C.; Singh, M. Structural and magnetic properties of nano nickel–zinc ferrite synthesized by reverse micelle technique. *J. Magn. Magn. Mater.* **2009**, *321*, 1–7. [CrossRef]
97. Patil, S.A.; Mahajan, V.C.; Ghatage, A.K.; Lotke, S.D. Structure and magnetic properties of Cd and Ti/Si substituted cobalt ferrites. *Mater. Chem. Phys.* **1998**, *57*, 86–91. [CrossRef]
98. Maji, P.; Choudhary, R.B. Facile synthesis, dielectric properties and electrocatalytic activities of PMMA-$NiFe_2O_4$ nanocomposite. *Mater. Chem. Phys.* **2017**, *193*, 391–400. [CrossRef]
99. Paswan, S.K.; Kumari, S.; Kar, M.; Singh, A.; Pathak, H.; Borah, J.P.; Kumar, L. Optimization of structure-property relationships in nickel ferrite nanoparticles annealed at different temperature. *J. Phys. Chem. Solids* **2021**, *151*, 109928. [CrossRef]
100. Nathani, H.; Gubbala, S.; Misra, R.D.K. Magnetic behavior of nanocrystalline nickel ferrite: Part I. The effect of surface roughness. *Mater. Sci. Eng. B* **2005**, *121*, 126–136.
101. Arumugham, N.; Mariappan, A.; Eswaran, J.; Daniel, S.; Kanthapazham, R.; Kathirvel, P. Nickel ferrite-based composites and its photocatalytic applications: A review. *J. Hazard. Mater. Adv.* **2022**, *8*, 100156. [CrossRef]
102. Chavan, A.R.; Chilwar, R.R.; Kharat, P.B.; Jadhav, K.M. Effect of annealing temperature on structural, morphological, optical and magnetic properties of $NiFe_2O_4$ thin films. *J. Supercond. Nov. Magn.* **2018**, *31*, 2949–2958. [CrossRef]
103. Salih, S.J.; Mahmood, W.M. Review on magnetic spinel ferrite (MFe_2O_4) nanoparticles: From synthesis to application. *Heliyon* **2023**, *9*, e16601. [CrossRef] [PubMed]
104. Kefeni, K.K.; Mamba, B.B. Photocatalytic application of spinel ferrite nanoparticles and nanocomposites in wastewater treatment: Review. *Sustain. Mater. Technol.* **2020**, *23*, e00140. [CrossRef]
105. da Silva, F.G.; Depeyrot, J.; Campos, A.F.C.; Aquino, R.; Fiorani, D.; Peddis, D. Structural and magnetic properties of spinel ferrite nanoparticles. *J. Nanosci. Nanotechnol.* **2019**, *19*, 4888–4902. [CrossRef] [PubMed]

106. Gasser, A.; Karim, M.; El-Gendy, A.A. Feasibility of superparamagnetic $NiFe_2O_4$ and GO–$NiFe_2O_4$ nanoparticles for magnetic hyperthermia. *Mater. Sci. Eng. B* **2023**, *297*, 116721.
107. Bibes, M.; Barthélémy, A. Oxide spintronics. *IEEE Trans. Electron Devices* **2007**, *54*, 1003–1023. [CrossRef]
108. Lüders, U.; Barthélémy, A.; Bibes, M.; Bouzehouane, K.; Fusil, S.; Jacquet, E.; Contour, J.-P.; Bobo, J.-F.; Fontcuberta, J.; Fert, A. $NiFe_2O_4$: A Versatile Spinel Material Brings New Opportunities for Spintronics. *Adv. Mater.* **2006**, *18*, 1733–1736. [CrossRef]
109. Ramos, R.; Kikkawa, T.; Uchida, K.; Adachi, H.; Lucas, I.; Aguirre, M.H.; Algarabel, P.A.; Morellón, L.; Maekawa, S.; Saitoh, E.; et al. Observation of the spin Seebeck effect in epitaxial Fe_3O_4 thin films. *Appl. Phys. Lett.* **2013**, *102*, 072413. [CrossRef]
110. Fetisov, Y.K.; Srinivasan, G. Electric field tuning characteristics of a ferrite-piezoelectric microwave resonator. *Appl. Phys. Lett.* **2006**, *88*, 143503. [CrossRef]
111. Srinivasan, G. Magnetoelectric composites. *Annu. Rev. Mater. Res.* **2010**, *40*, 153–178. [CrossRef]
112. Binek, C.; Doudin, B. Magnetoelectronics with magnetoelectrics. *J. Phys. Condens. Matter* **2005**, *17*, L39–L44. [CrossRef]

Disclaimer/Publisher's Note: The statements, opinions and data contained in all publications are solely those of the individual author(s) and contributor(s) and not of MDPI and/or the editor(s). MDPI and/or the editor(s) disclaim responsibility for any injury to people or property resulting from any ideas, methods, instructions or products referred to in the content.